IEEE Access
Multidisciplinary ⋮ Rapid Review ⋮ Open Access Journal

Received October 24, 2019, accepted November 12, 2019, date of publication November 21, 2019,
date of current version December 6, 2019.

Digital Object Identifier 10.1109/ACCESS.2019.2954858

Hidden Vehicle Sensing via Asynchronous V2V Transmission: A Multi-Path-Geometry Approach

KAIFENG HAN[1], SEUNG-WOO KO[2], (Member, IEEE), HYUKJIN CHAE[3], BYOUNG-HOON KIM[4], AND KAIBIN HUANG[5], (Senior Member, IEEE)

[1]Institute of Policy and Economics Research, China Academy of Information and Communications Technology, Beijing 100191, China
[2]Division of Electronics and Electrical Information Engineering, Korea Maritime and Ocean University, Busan 49112, South Korea
[3]Independent Researcher, USA
[4]LG Electronics, Seoul 06772, South Korea
[5]Department of Electrical and Electronic Engineering, The University of Hong Kong, Hong Kong

Corresponding author: Seung-Woo Ko (swko@kmou.ac.kr)

This work was supported in part by the Basic Science Research Program through the National Research Foundation of Korea (NRF) funded by the Ministry of Science and ICT (NRF-2019R1G1A1100123), in part by the Hong Kong Research Grants Council under the Grant 17208319, Grant 17209917, and Grant 17259416, and in part by LG Electronics.

ABSTRACT Accurate vehicular sensing is a basic and important operation in autonomous driving. Unfortunately, the existing techniques have their own limitations. For instance, the communication-based approach (e.g., transmission of GPS information) has high latency and low reliability while the reflection-based approach (e.g., RADAR) is incapable of detecting *hidden vehicles* (HVs) without line-of-sight. This is arguably the reason behind some recent fatal accidents involving autonomous vehicles. To address this issue, this paper presents a novel HV-sensing technology that exploits multi-path transmission from a HV to a *sensing vehicle* (SV). The powerful technology enables the SV to detect multiple HV-state parameters including position, orientation of driving direction, and size. Its implementation does not even require synchronization like conventional mobile positioning techniques. Our design approach leverages estimated information on multi-path [namely their *angles-of-arrival* (AoA), *angles-of-departure* (AoD), and *time-of-arrival* (ToA)] and their geometric relations. As a result, a complex system of equations or optimization problems, where the desired HV-state parameters are variables, can be formulated for different channel-noise conditions. The development of intelligent solution methods ranging from least-square estimator to disk/box minimization yields a set of practical HV-sensing techniques. We study their feasibility conditions in terms of the required number of paths. Furthermore, practical solutions, including sequential path combining and random directional beamforming, are proposed to enable HV-sensing given insufficient paths. Last, realistic simulation of driving in both highway and rural scenarios demonstrates the effectiveness of the proposed techniques. In summary, the proposed technique will enhance the capabilities of existing vehicular sensing technologies (e.g., RADAR and LIDAR) by enabling HV-sensing.

INDEX TERMS Hidden vehicle sensing, asynchronous V2V transmission, NLoS positioning, multi-path geometry.

I. INTRODUCTION

Autonomous driving (auto-driving) aims at reducing car accidents, traffic congestion, and greenhouse gas emissions by automating the transportation process [2]. The potential impact of the cross-disciplinary technology has attracted heavy R&D investments not only by leading car manufacturers (e.g., Tesla) but also Internet companies (e.g., Google). One primary operation of auto-driving is vehicular positioning [3]–[5], namely positioning nearby vehicles and tracking other parameters such as sizes and trajectories. The information then serves as inputs for computing and control tasks

The associate editor coordinating the review of this manuscript and approving it for publication was Huan Zhou.

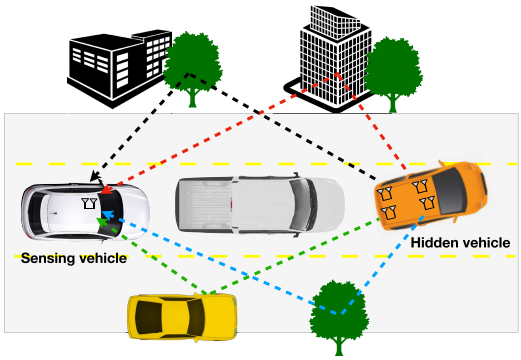

FIGURE 1. Hidden vehicle scenario with multi-path NLoS channels.

such as navigation [6], accidence avoidance [7], and an electric vehicle's battery changing [8]. There exist diversified approaches for vehicular positioning but they all have their own drawbacks. One conventional approach is to exchange the absolute location information among a group of nearby vehicles by using *vehicle-to-vehicle* (V2V) transmission [9]. Its main drawbacks include high latency due to the data exchanging process and low reliability arising from inaccurate *Global Positioning System* (GPS) information in e.g., dense urban areas or tunnels [2]. Another approach is to deploy sensors ranging from *LIght Detection and Ranging* (LIDAR) to *RAdio Detection And Ranging* (RADAR). As illustrated in Fig. 1, they are capable of sensing the *line-of-sight* (LoS) vehicles, but cannot "see through" a large solid object (e.g., a truck) to detect *hidden vehicles* (HVs). A comprehensive discussion of existing approaches is given in the sequel. Motivated by their drawbacks, this paper presents a novel technology for accurately sensing a HV including detecting its position, orientation of driving direction, and size by exploiting the multi-path geometry of asynchronous V2V transmission.

A. WIRELESS TRANSMISSION AND VEHICULAR POSITIONING

Wireless transmission underpins different approaches for vehicular positioning as follows.

1) COMMUNICATION-BASED VEHICULAR POSITIONING

Nearby vehicles can position each other by *vehicle-to-everything* (V2X) communication to exchange GPS information [9]. The state-of-the-art protocol for connecting vehicles is the low-latency *dedicated short-range communication* (DSRC) [10], a variant of the IEEE 802.11 Wi-Fi random-access protocol. The effectiveness of the protocol has been examined in the scenario of two-lane rural highway [11]. Recently, *the 3rd Generation Partner Project* (3GPP) has initiated a standardization process to realize *cellular-based V2X* (C-V2X) communication supporting higher data rate and larger coverage than DSRC [12]. To boost data rate, the technology aims at implementation in the *millimetre-wave* (mmWave) spectrum where abundant of bandwidth is available [13]. A key challenge faced by mmWave V2X communication is the high overhead arising from frequent ultra-sharp beam training and alignment to cope with fast fading in channels between high-speed vehicles. To reduce this overhead, a fast beam-alignment scheme is proposed in [14] that leverages matching theory and swarm intelligence to efficiently pair vehicles. An alternative technique for accelerating beam alignment is to leverage information generated by either onboard RADAR [15] or GPS [16] to deduce useful channel information.

The main challenge faced by the communication-based approach is that their reliability and latency may not meet the requirements of mission-critical scenarios such as accident avoidance at high speeds. Consider the reliability issue. The GPS information exchanged between vehicles can be highly inaccurate due to the blockage of GPS signals from satellites in urban areas or tunnels. Next, consider the latency issue. The implementation of V2X communication in a dense vehicular network incurs high communication overhead due to many practical factors including complex protocols, packet loss and retransmission, source and channel coding, limited link life time, etc. The long latency makes relevant positioning information easily out-of-date [17]. Due to the above issues, the application of the communication-based approach is limited to pedestrian positioning but not yet suitable for a latency-sensitive task like vehicular positioning.

2) REFLECTION-BASED VEHICULAR POSITIONING

Auto-driving vehicles are typically equipped with RADAR and LIDAR among other sensing devices. The two sensing technologies both adopt the reflection-based approach, namely that the sensors detect the reflections from vehicles and objects in the environment but using different mediums, microwaves and laser light, respectively.

LIDAR steers ultra-sharp laser beams to scan the surrounding environment and generates a dynamic high-resolution *three-dimensional* (3D) map for navigation [18]. The main drawback of LIDAR is its ineffectiveness under hostile weather conditions due to the difficulty of light in penetrating fog, snow, and rain [2]. In addition, LIDAR is currently too expensive to be practical and the huge amount of generated data is challenging to be processed within the ultra-low latency required for safe driving.

RADAR can locate a target object as well as estimate its velocity via sending a designed waveform [e.g., *frequency modulated continuous waveform* (FMCW)] and analyzing its reflection by the object [19]. Particularly, the metal surfaces of vehicles are capable of reflecting microwaves with negligible absorption. For the reason, RADAR is popularly used for long-range sensing. Recent breakthroughs in mmWave RADAR make it feasible to deploy large-scale but high impact arrays for sharp beamforming to achieve a high positioning accuracy [20]. Compared with LIDAR, RADAR can provide longer sensing ranges (up to hundreds-of-meter) and

retain the effectiveness under hostile weather conditions or in an environment with poor lighting. One disadvantage of RADAR is that it may incorrectly recognize a harmless small metal object as a much larger object due to scattering, leading to false alarms [21].

In the context of auto-driving, perhaps the most critical limitation of LIDAR, RADAR and other reflection-based technologies is that they can detect only vehicles with LoS since neither microwaves nor laser light can penetrate a large solid object such as a truck or a building. However, detecting HVs with *non-LoS* (NLoS) is crucial for collision avoidance in complex scenarios such as overtaking and cross junctions as illustrated in Fig. 1.

B. LOCALIZATION BY SYNCHRONOUS TRANSMISSION

Besides to vehicular positioning, there exists an active research area to estimate the positions of mobile devices in cellular networks, a. k. a. *localization* [22], most of which rely on *synchronous* transmissions. For example, a receiver (e.g., a mobile device) estimates the relative position of a transmitter [e.g., *base station* (BS)] from the prior knowledge of the transmitted waveform (see e.g., [22], [23]). The effectiveness of this approach hinges on the key assumption of perfect synchronization between the transmitter and receiver. The reason is that the *distance* of each propagation path can be directly converted from its *propagation delay*, i.e., *Time-of-Arrival* (ToA) (for pulse transmission) [24] or *frequency variation* (for FMCW transmission) [25], which can be easily measured given the said synchronization. Localization via asynchronous transmission is possible when *received-signal-strength* (RSS) information is given [26], but the resultant accuracy is far from that via synchronous transmission. On the other hand, spatial parameters of individual paths, including the AoA and AoD, can be estimated if the transmitter and receiver are equipped with antenna arrays to perform spatial filtering [27]. Combining the distances and spatial parameters of multi-paths and exploiting their geometric relations enable the localization despite the lack of LoS, given the perfect *synchronization among multiple transmitters* [24], [28], [29].

The assumption of perfect transmitter-receiver or transmitter-transmitter synchronizations is reasonable for localization in cellular networks since the BSs and mobiles are relatively stationary. However, in the auto-driving scenario, the transmitter and receiver are a HV and a *sensing vehicle* (SV), respectively, and their synchronization is impractical especially at high speeds.[1] This renders the approach based on synchronous transmission unsuitable for vehicular positioning. In view of the prior work, sensing a HV remains largely an open problem and tackling it is the theme of this work.

[1]The synchronization error for wireless communications is typically around $\pm 0.39\mu$ sec [30], which is negligible compared with the size of a cyclic prefix (4.7μ sec). However, from a positioning perspective, this synchronization error will result in ± 117 (m) distance error, which is unacceptable and thus calls for developing a positioning technique without transmitter-receiver synchronization.

C. MAIN CONTRIBUTIONS

In this work, we aim at tackling the open challenges faced by existing vehicular positioning techniques as summarized below.

1) **No LoS and lack of synchronization:** None of the existing techniques (see Table 1) can be effective for sensing a HV that has *neither LoS nor synchronization* (with the SV).

2) **Simultaneous detection of HV's position, orientation, and size:** Except for LIDAR, other existing vehicular positioning approaches are incapable of detecting the size and orientation of a HV, which are important safety information required in auto-driving. For auto-driving safety, all of the vehicle's safety information (position, orientation, and size) should be given simultaneously but the existing technologies cannot guarantee to achieve the goal due to various practical factors, e.g., GPS-denied environments, high mobility, and the perfect alignment among them.

3) **Insufficient multi-path:** Similar to the approach based on synchronous transmission, the current technology positions a HV by exploiting multi-path propagation. Such approaches may not be feasible in the scenario with sparse scattering and hence insufficient paths. Tackling the challenge is important for making the technologies robust.

To tackle the above challenges, we propose a novel technology, called HV-sensing, to enable a SV to simultaneously sense the position, orientation of driving direction, and size of a HV without requiring synchronization. The SV leverages the information of multi-path signals (including AoA, AoD, and ToA) as well the derived geometry relations between the paths so as to construct tractable systems of equations or optimization problems, where the HV position, orientation of driving direction, and size are unknown variables to be found. A set of HV-sensing techniques is designed for operation in different practical settings ranging from low to high *signal-to-noise ratios* (SNRs), single-cluster to multi-cluster HV arrays, and small to large waveform sets. The differences between the proposed HV-sensing technology and conventional approaches are summarized in Table 1.

The proposed vehicular sensing technique can be used to assist and enhance the current positioning approaches by overcoming their limitations as well as enabling the vehicle to sense the state of a HV including detecting its position, orientation, and size. This technique can be integrated with current vehicular positioning system to further improving safety of auto-driving. The main contributions of this work are summarized as follows.

1) **Sensing HV position and orientation by using single cluster array:** Consider the case that the HV array contains a cluster of collocated antennas. The goal is to simultaneously estimate HV's position and orientation without SV-HV synchronization. The HV transmits orthogonal waveforms over different antennas, enabling the SV to estimate the multi-path information (AoA, AoD, and ToA). This multi-path transmission allows the SV to resolve the synchronization issues as follows. First, all signal paths are simultaneously originated from the HV, providing the same effect of being

TABLE 1. Comparison of different vehicular positioning approaches.

Approach	Require LoS?	Require Sync.?	Size Detection	Reliability
Communication-Based	No	Yes	×	Low (GPS dependent)
Reflection-Based	Yes	Yes	LIDAR: ✓ RADAR ×	Low (environment dependent)
Synchronous Transmission	No	Yes	×	Low (need sync.)
HV-Sensing (proposed)	No	No	✓	High

perfectly synchronized among different signal paths. Second, the SV can calculate the *Time-Difference-of-Arrival* (TDoA) between any two signal paths from the observed ToAs even in the absence of HV-SV synchronization, which is proportional to the corresponding flight distance difference. Given the three-fold information (AoA, AoD, and TDoA) and when noise is negligible, a complex system of equations is constructed and solved in sequential steps at SV to obtain the desired HV-state parameters. On the other hand, when noise is present, the sensing problem is reformulated as *least-square* (LS) estimation also solved in a sequential procedure. For the HV sensing to be feasible, the required numbers of paths are at least 4 in 2D propagation (see Proposition 1) and 3 in 3D propagation (see Proposition 3).

2) **Sensing HV size by using multiple clusters array:** Consider the case that the HV array contains multiple clusters of antennas that are distributed over the vehicular body. In this case, the goal is to further estimate the HV size along with its position and orientation. Two specific schemes are presented. The first assumes the transmission of multiple orthogonal waveform sets so that the SV can group the paths according to their originating HV antenna clusters. The second assumes the transmission of an identical waveform set such that the said path-grouping is infeasible. Then alternative size detection techniques are proposed based on efficient disk or box minimization under the constraint that the disk or box encloses the HV array. The required numbers of paths for the first sensing scheme is found to be 6 and that for the second scheme is 4. Nevertheless, when both of two schemes are feasible, the former outperforms the latter as multiple orthogonal waveform sets help to improve sensing accuracy.

3) **Coping with insufficient multi-path:** To make the proposed HV-sensing techniques more reliable, we further propose practical solutions for increasing the number of available paths in the case when there are insufficient for meeting the feasibility requirements of the above HV-sensing techniques. The first solution is to *combine paths* exploited in multiple time instants and the second is to apply random directional beamforming for uncovering *hidden paths* invisible in the case of isotropic HV transmission. The solutions are complementary and can be jointly implemented to maximize the number of significant paths for enhancing the sensing accuracy.

4) **Realistic simulation:** The proposed HV-sensing techniques are evaluated using practical simulation models of highway and rural scenarios and found to be effective.

The remainder of the paper is organized as follows. Section II introduces the system model and problem formulation for HV-sensing. Sections III and IV present the HV-sensing techniques for the cases of single-cluster and multi-cluster HV arrays, respectively. The solutions for the practical issue of insufficient multi-path for HV-sensing are developed in Section V, and the extension to the multi-vehicle scenario is considered in VI. Simulation results are presented in Section VII, followed by concluding remarks in Section VIII.

II. SYSTEM MODEL

We consider a two-vehicle system where a SV attempts to detect the (relative) position, size, and orientation of a HV. An antenna cluster refers to a set of *collocated* antennas where the half-wavelength antenna spacing is negligible compared with vehicle sizes and propagation distances. An array can comprise single or multiple antenna clusters, referred to as a *single-cluster* array and a *multi-cluster* array, respectively. The deployment of a single-cluster array at the HV enables the SV to detect the HV's position and orientation. On the other hand, a multi-cluster HV array can further make it possible for the SV to estimate the HV size. For the exposition, in the case of multi-cluster HV array, we consider 4 clusters located at the vertices of a rectangle representing the vehicle. The principle of HV-sensing design in the sequel is based on the efficient detection of the clusters' positions and thus can be straightforwardly extended to other clusters' topologies with irregular clusters' distributions. For HV-sensing in both scenarios, the SV requires only a single-cluster array. Signal propagation is assumed to be contained in the 2D plane, and the results are subsequently extended to the 3D propagation. The channel model, V2V transmission, and sensing problem are described in the following sub-sections.

A. MULTI-PATH NLoS CHANNEL

The NLoS channel between SV and HV contains multi-paths reflected by a set of scatterers. Consider the characteristics of V2V channel [31]. We make the following assumption.

Assumption 1 (Single-Bounce Scattering): The single-bounce scattering is used to model the V2V propagations that the NLoS signals are assumed to have only one reflection due to scatterers.[2]

[2]Assumption 1 is widely used in the literature of localization via NLoS paths [23], [27]. Various methods have been proposed to detect single-bounce paths among multiple-bounce ones such a proximity detection [27], and a joint ToA-and-signal strength based detection [32], making sense to use Assumption 1 in practice.

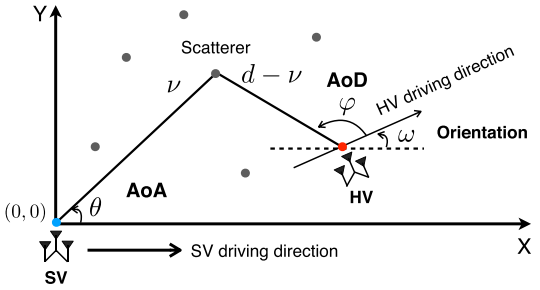

FIGURE 2. The geometry of a 2D propagation path and the definitions of parameters.

Based on Assumption 1, a 2D Cartesian coordinate system is considered as illustrated in Fig. 2, where the SV array is located at the origin and the X-axis is aligned with the orientation of SV. Further, consider a typical antenna cluster at the HV. Each NLoS signal path from the HV antenna cluster to the SV array can be characterized by the following five parameters: the AoA at the SV denoted by θ; the AoD at the HV denoted by φ; the orientation of the HV denoted by ω; and the propagation distance denoted by d which is divided into the propagation distance after reflection, denoted by ν, and the remaining distance $(d-\nu)$. The AoD and AoA are defined as azimuth angles relative to orientations of HV and SV, respectively. Fig. 2 graphically shows the definitions of the above parameters.

B. HIDDEN VEHICLE TRANSMISSION

To enable sensing at the SV, the HV transmits a set of waveforms defined as follows. Each antenna cluster at HV has M_t antennas with at least half-wavelength spacing between adjacent antennas. Consider a typical antenna cluster. A set of orthogonal waveforms are transmitted over different antennas.[3] Let $s_m(t)$ be the finite-duration baseband waveform in $t \in [0, T_s]$ assigned to the m-th HV antenna with the bandwidth B_s. Then the waveform orthogonality is specified by $\int_0^{T_s} s_{m_1}(t)s^*_{m_2}(t)dt = \delta(m_1 - m_2)$ with the delta function $\delta(x) = 1$ if $x = 0$ and 0 otherwise. The transmitted waveform vector for the k-th HV antenna cluster is $\mathbf{s}^{(k)}(t) = [s_1^{(k)}(t), \cdots, s_{M_t}^{(k)}(t)]^{\mathrm{T}}$. In the case of multi-cluster HV array, the waveform sets for different clusters are either *identical* or *orthogonal* with each other. The use of orthogonal waveform sets allows SV to group the detected paths according to their originating antenna clusters as elaborated in the sequel, and hence this case is referred to as *decoupled clusters*. Then the other case is called *coupled clusters*. With the prior knowledge of transmitted waveforms, the SV with M_r antennas can scan the received signal due to the HV transmission to resolve multi-path as discussed in the next sub-section.

[3]It is implicitly assumed that enough orthogonal waveforms are given for HV's multi-antenna transmission a.k.a. *orthogonal multiple access* (OMA). It is interesting to extend the current design to *non-orthogonal multiple access* (NOMA) [33] against case of insufficient orthogonal waveforms, which is outside the scope of current work.

The expression of the received signal is obtained as follows. Consider a typical HV antenna cluster. Based on the far-field propagation model, the cluster response vector is a function of the AoD φ defined as

$$\mathbf{a}(\varphi)=[\exp(j2\pi f_c\alpha_1(\varphi)), \cdots, \exp(j2\pi f_c\alpha_{M_t}(\varphi))]^{\mathrm{T}}, \quad (1)$$

where f_c denotes the carrier frequency and $\alpha_m(\varphi)$ is the propagation time difference between received signals departing from the HV's m-th antenna and the first antenna, i.e., $\alpha_1(\varphi) = 0$. The response vector of the SV array is written in terms of AoA θ as

$$\mathbf{b}(\theta) = [\exp(j2\pi f_c\beta_1(\theta)), \cdots, \exp(j2\pi f_c\beta_{M_r}(\theta))]^{\mathrm{T}}, \quad (2)$$

where $\beta_m(\theta)$ refers to the propagation time difference between received signals arriving at the SV's m-th antenna and the first antenna. We assume that SV has prior knowledge of both the HV-and-SV array configurations and thereby the response functions $\mathbf{a}(\varphi)$ and $\mathbf{b}(\theta)$. This is feasible by standardizing the vehicular arrays' topology. In addition, the Doppler effect is ignored based on the assumption that the channel coherence time due to Doppler frequency shift is much larger than the waveform duration and thus does not affect waveform orthogonality (see Remark 1). Let k denote the index of HV antenna cluster and $P^{(k)}$ denote the number of received paths originating from the k-th HV antenna cluster. The total number of paths arriving at SV is $P = \sum_{k=1}^{K} P^{(k)}$. We represent the received signal vector at SV as $\mathbf{r}(t) = [r_1(t), \cdots, r_{M_r}(t)]^{\mathrm{T}}$ that can be written in terms of $\mathbf{s}(t)$, $\mathbf{a}(\varphi)$ and $\mathbf{b}(\theta)$ as

$$\mathbf{r}(t) = \sum_{k=1}^{K}\sum_{p=1}^{P^{(k)}} \gamma_p^{(k)}\mathbf{b}\left(\theta_p^{(k)}\right)\mathbf{a}^{\mathrm{T}}\left(\varphi_p^{(k)}\right)\mathbf{s}\left(t-\lambda_p^{(k)}\right)+\mathbf{n}(t),$$

where $\gamma_p^{(k)}$ and $\lambda_p^{(k)}$ denote the complex channel coefficient and ToA of path p originating from the k-th HV antenna cluster, respectively, and $\mathbf{n}(t)$ represents channel noise. With *no synchronization* between the HV and SV, the SV has no information of HV's transmission timing. Therefore, it is important to note that $\lambda_p^{(k)}$ differs from the corresponding propagation delay, denoted by $\tau_p^{(k)}$, with $\tau_p^{(k)} = \frac{d_p^{(k)}}{c}$ and $d_p^{(k)}$ being the propagation distance. Given an unknown clock-synchronization gap between the HV and SV denoted as Γ, $\tau_p^{(k)} = \lambda_p^{(k)} - \Gamma$.

Remark 1 (Channel Coherence Time vs. Waveform Duration): It is essential to study the condition on channel dynamics for accurate and stable positioning. Specifically, the assumption of invariant ToA, AoA and AoD holds if the V2V channel is largely unchanged in the waveform duration:

$$T_c \gg T_w, \quad (3)$$

where T_c and T_w denote the channel coherence time and waveform duration, respectively. To verify the condition, we analyze the two metrics as follows.

- *Coherence Time:* It is well-known that T_c is inversely proportional to the maximum Doppler frequency f_Δ as

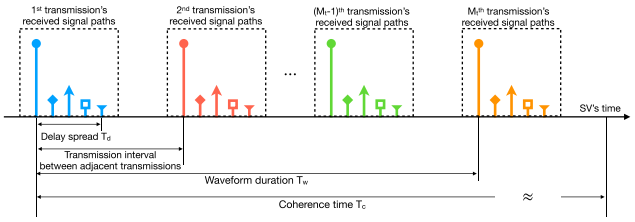

FIGURE 3. The relation among delay spread, waveform duration, and coherence time. A Fourier matrix is selected as a reference signal of the waveform of which the length is the number of transmit antenna M_t.

$T_c \approx \frac{1}{f_\Delta} = \frac{c}{f_c v}$ with the relative velocity of HV to SV v (HV and SV are driving in in opposite directions) and the carrier frequency f_c. When $v = 200$ (km/h) and $f_c = 5.9$ (GHz), T_c approximately becomes 0.9153 (msec).

- *Waveform Duration:* We select a M_t by M_t Fourier matrix as a codeword of the orthogonal waveform [34]. To guarantee the waveform's orthogonality, the interval between adjacent code transmissions should be larger than the channel's delay-spread, denoted by T_d, enabling to avoid inter-code interference (see Fig. 3). In other words, we should satisfy $T_w \geq M_t T_d$, where M_t refers to the length of the codeword. Note the coverage of V2V channel with $f_c = 5.9$ (GHz) is less than 1 (km) [35], which is translated to the maximum delay spread $\frac{10^3}{c} \approx 3.33$ (μsec). Given $M_t = 20$, we obtain $T_w \geq 0.0667$ (msec).

As a result, the condition in (3) is satisfied. It is worth mentioning that the technique proposed in the sequel is based on this *one-way* transmission of which the entire duration is significantly shorter than conventional two-way positioning approaches (e.g., *round-trip-time* (RTT) based), enabling accurate and stable positioning in highly dynamic environments.

C. ESTIMATIONS OF AoA, AoD, AND ToA

The sensing techniques in the sequel assume that the SV has the knowledge of AoA, AoD, and ToA of each receive NLoS signal path, say path p, denoted by $\{\theta_p, \varphi_p, \lambda_p\}$ where $p \in \mathcal{P} = \{1, 2, \cdots, P\}$. The knowledge can be acquired by applying classical parametric estimation techniques briefly described as follows.

1) Sampling: The received analog signal $\mathbf{r}(t)$ and the waveform vector $\mathbf{s}(t)$ are sampled at the Nyquist rate B_s and converted to the digital signal vectors $\mathbf{r}[n]$ and $\mathbf{s}[n]$, respectively.

2) Matched Filter: The sequence of $\mathbf{r}[n]$ is matched-filtered by $\mathbf{s}[n]$. The resultant $M_r \times M_t$ coefficient matrix $\mathbf{Y}[z]$ is given by $\mathbf{Y}[z] = \sum_n \mathbf{r}[n]\mathbf{s}^H[n - z]$. The sequence of ToAs $\{\lambda_p\}$ can be estimated by detecting peak points of the matrix norm $\|\mathbf{Y}[z]\|$, denoted by $\{z_p\}$, which can be converted into time by multiplication with the time resolution $\frac{1}{B_s}$. One peak point can contain multiple signal paths if the signals arrive within the same sampling interval.

3) Multi-Path Estimation: Given $\{\mathbf{Y}[z_p]\}$, AoAs and AoDs are jointly estimated by scanning two-dimensions angular domains by leveraging the prior knowledge of $\mathbf{a}(\varphi)$ in (1) and $\mathbf{b}(\theta)$ in (2). It is called a 2D-*multiple signal classification* (MUSIC) algorithm, which is the most widely used subspace-based detection method. The estimated AoA $\{\theta_p\}$ and AoD $\{\varphi_p\}$ are paired with the corresponding estimated ToA $\{\lambda_p\}$, which jointly characterize path p.

It is worth mentioning that only a small portion of signal paths can be observed among the entire ones because some of them experience severe signal attenuations due to path-loss and small-scale fading and their received signal strengths are not enough to estimate AoD/AoA accurately.

D. HIDDEN VEHICLE SENSING PROBLEM

The SV attempts to sense the HV's position, size, and orientation, which can be obtained by using parameters of AoA θ, AoD φ, orientation ω, distances d and v, and location of multi-cluster HV array.[4] Noting the first two parameters are obtained based on the estimations in Section II-C and the goal is to estimate the remaining parameters.

III. SENSING HIDDEN VEHICLE WITH A SINGLE-CLUSTER ARRAY

In this section, we consider the scenario that a single-cluster array is deployed at HV. Then this section focuses on designing the sensing techniques for SV to detect 1) the HV position (i.e., position of the single-cluster array), specified by the coordinate $\mathbf{p} = (x, y)$, and 2) the HV orientation, specified by ω (see Fig. 2). Based on the multi-path-geometry, $\mathbf{p}$ is described as

$$\begin{cases} x = \nu_p \cos(\theta_p) - (d_p - \nu_p)\cos(\varphi_p + \omega), \\ y = \nu_p \sin(\theta_p) - (d_p - \nu_p)\sin(\varphi_p + \omega), \end{cases} \quad \forall p \in \mathcal{P}. \quad (4)$$

The prior knowledge that SV has for sensing is the parameters of P NLoS paths estimated as described in Section II-C. Each path, say path p, is determined by the parametric set $\{\theta_p, \phi_p, \lambda_p\}$ and orientation ω as (4) shows. Then given the equations in (5), the **sensing problem** for the current scenario reduces to

$$\bigcup_{p \in \mathcal{P}} \{\theta_p, \phi_p, \lambda_p\} \Rightarrow \{\mathbf{p}, \omega\}. \quad (5)$$

A. SENSING FEASIBILITY CONDITION

In this subsection, it is shown that for the HV-sensing to be feasible, there should exist at least *four* NLoS paths. To this end, by using (4) and multi-path-geometry, we can obtain the following system of equations:

$$\begin{cases} x_p = \nu_p \cos(\theta_p) - (d_p - \nu_p)\cos(\varphi_p + \omega) \\ \quad = \nu_1 \cos(\theta_1) - (d_1 - \nu_1)\cos(\varphi_1 + \omega), \\ y_p = \nu_p \sin(\theta_p) - (d_p - \nu_p)\sin(\varphi_p + \omega) \\ \quad = \nu_1 \sin(\theta_1) - (d_1 - \nu_1)\sin(\varphi_1 + \omega), \end{cases} \quad p \in \mathcal{P}, \text{ (E1)}$$

[4]The proposed sensing technique is to exploit the geometry relation between a few channel parameters of a signal path i.e., TDoA/AoA/AoD, which is analogy to transmitting a reference signal for conventional wireless channel estimation (e.g., [36]).

where (x_p, y_p) denotes the coordinate characterized via path p. The number of equations in E1 is $2(P-1)$, and the above system of equations has a unique solution when the dimensions of unknown variables are less than $2(P-1)$. Since the AoAs $\{\theta_p\}$ and AoDs $\{\varphi_p\}$ are known, the number of unknowns is $(2P+1)$ including the propagation distances $\{d_p\}$, $\{v_p\}$, and orientation ω. To further reduce the number of unknowns, we use the propagation time difference between signal paths also known as TDoAs, denoted by $\{\rho_p\}$, which can be obtained from the difference of ToAs as $\rho_p = \lambda_p - \lambda_1$ where $\rho_1 = 0$. The propagation distance of signal path p, say d_p, is then expressed in terms of d_1 and ρ_p as

$$d_p = c(\lambda_p - \Gamma) = c(\lambda_1 - \Gamma) + c(\lambda_p - \lambda_1) = d_1 + c\rho_p, \quad (6)$$

for $p \in \{2, \cdots, P\}$. Substituting the above $(P-1)$ equations into E1 eliminates the unknowns $\{d_2, \cdots, d_P\}$ and hence reduces the number of unknowns from $(2P+1)$ to $(P+2)$. As a result, E1 has a unique solution when $2(P-1) \geq P+2$.

Proposition 1 (Sensing Feasibility Condition): To sense the position and orientation of a HV equipped with a single-cluster array, at least four NLoS signal paths are required: $P \geq 4$.

Remark 2 (Asynchronization): Recall that one sensing challenge is asynchronization between HV and SV represented by Γ, which is a latent variable we cannot observe explicitly. In our proposed approach, based on the fact that all NLoS paths experience the same synchronization gap, we do not need to consider Γ in the positioning procedure.

B. HIDDEN VEHICLE SENSING WITHOUT NOISE

Consider the case of a high receive *signal-to-noise ratio* (SNR) where noise can be neglected, i.e., the estimations of AoA/AoD/ToA $\{\theta_p, \phi_p, \lambda_p\}$ are perfect. Then the HV-sensing problem in (5) is translated to solve the system of equations in E1. One challenge is that the unknown orientation ω introduces nonlinear relations, namely $\cos(\varphi_p + \omega)$ and $\sin(\varphi_p + \omega)$, in the equations. To overcome the difficulty, we adopt the following two-step approach: 1) estimate the correct orientation ω^* via its discriminant introduced in the sequel; 2) given ω^*, the equation becomes linear and thus can be solved via LS estimator, giving the position $\mathbf{p}^*$. To this end, the equations in E1 can be arranged in a matrix form as

$$\mathbf{A}(\omega)\mathbf{z} = \mathbf{B}(\omega), \quad \text{(E2)}$$

where $\mathbf{z} = (\mathbf{v}, d_1)^{\mathrm{T}} \in \mathbb{R}^{(P+1)\times 1}$ and $\mathbf{v} = \{v_1, \cdots, v_P\}$. For matrix $\mathbf{A}(\omega)$, we have

$$\mathbf{A}(\omega) = \begin{bmatrix} \mathbf{A}^{(\cos)}(\omega) \\ \mathbf{A}^{(\sin)}(\omega) \end{bmatrix} \in \mathbb{R}^{2(P-1)\times(P+1)}, \quad (7)$$

where $\mathbf{A}^{(\cos)}(\omega)$ is

$$\begin{bmatrix} a_1^{(\cos)} & -a_2^{(\cos)} & 0 & \cdots & 0 & a_{1,2}^{(\cos)} \\ a_1^{(\cos)} & 0 & -a_3^{(\cos)} & \cdots & 0 & a_{1,3}^{(\cos)} \\ \vdots & \vdots & \vdots & \ddots & \vdots & \vdots \\ a_1^{(\cos)} & 0 & 0 & \cdots & -a_P^{(\cos)} & a_{1,P}^{(\cos)} \end{bmatrix} \quad (8)$$

with $a_p^{(\cos)} = \cos(\theta_p) + \cos(\varphi_p + \omega)$ and $a_{1,p}^{(\cos)} = \cos(\varphi_p + \omega) - \cos(\varphi_1 + \omega)$, and $\mathbf{A}^{(\sin)}(\omega)$ is obtained by replacing all cos operations in (8) with sin operations. Next,

$$\mathbf{B}(\omega) = \begin{bmatrix} \mathbf{B}^{(\cos)}(\omega) \\ \mathbf{B}^{(\sin)}(\omega) \end{bmatrix} \in \mathbb{R}^{2(P-1)\times 1}, \quad (9)$$

where $\mathbf{B}^{(\cos)}(\omega) = [c\rho_2 \cos(\varphi_2 + \omega), c\rho_3 \cos(\varphi_3 + \omega), \cdots, c\rho_P \cos(\varphi_P + \omega)]^{\mathrm{T}}$, and $\mathbf{B}^{(\sin)}(\omega)$ is obtained by replacing all cos in $\mathbf{B}^{(\cos)}(\omega)$ with sin.

1) Computing ω^*: Note that E2 becomes an *over-determined* linear system of equations if $P \geq 4$ (see Proposition 1), providing the following discriminant of orientation ω. Since the equations in (7) are based on the geometry of multi-path propagation and HV orientation as illustrated in Fig. 2, there exists a unique solution for the equations. Then we can obtain from (7) the following result, which is useful for computing ω^*.

Proposition 2 (Discriminant of Orientation): With $P \geq 4$, the unique ω^* exists when $\mathbf{B}(\omega^*)$ is orthogonal to the left null space of $\mathbf{A}(\omega^*)$ denoted by $\mathsf{null}(\mathbf{A}(\omega^*)^{\mathrm{T}}) \in \mathbb{R}^{2(P-1)\times(P-3)}$:

$$\mathsf{null}(\mathbf{A}(\omega^*)^{\mathrm{T}})^{\mathrm{T}}\mathbf{B}(\omega^*) = \mathbf{0}. \quad (10)$$

Proof: See Appendix A.

Given this discriminant, a simple 1D search can be performed over $[0, 2\pi]$ to find ω^*. Note that the computation complexity of the 1D search is low, and the method can be decomposed into multiple independent computations. As a result, the time to find ω^* can be significantly reduced, and it is possible to run the searching algorithm in real-time vehicular sensing scenarios.

2) Computing $\mathbf{p}^*$: Given the ω^*, E2 can be solved by

$$\mathbf{z}^* = \left[\mathbf{A}(\omega^*)^{\mathrm{T}}\mathbf{A}(\omega^*)\right]^{-1}\mathbf{A}(\omega^*)^{\mathrm{T}}\mathbf{B}(\omega^*). \quad (11)$$

Then the HV position $\mathbf{p}^*$ can be computed by substituting (10) and (11) into (6) and E1.

C. HIDDEN VEHICLE SENSING WITH NOISE

In the presence of significant channel noise, the estimated AoAs/AoDs/ToAs contain errors. Consequently, HV-sensing is based on the noisy versions of matrix $\mathbf{A}(\omega)$ and $\mathbf{B}(\omega)$, denoted by $\tilde{\mathbf{A}}(\omega)$ and $\tilde{\mathbf{B}}(\omega)$, which do not satisfy the equations in (E2) and (10). To overcome the difficulty, we develop a sensing technique by converting the equations into minimization problems whose solutions are robust against noise.

1) Computing ω^*: Based on (10), we formulate the following problem to find the orientation ω:

$$\omega^* = \arg\min_{\omega} \left[\mathsf{null}(\tilde{\mathbf{A}}(\omega)^{\mathrm{T}})^{\mathrm{T}}\tilde{\mathbf{B}}(\omega)\right], \quad (12)$$

Solving the problem relies on a 1D search over $[0, 2\pi]$.

2) Computing $\mathbf{p}^*$: Next, given ω^*, the optimal $\mathbf{z}^*$ can be derived by using the LS estimator that minimizes the squared

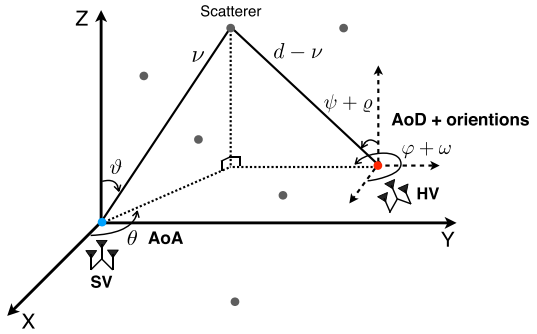

FIGURE 4. 3D propagation model.

Euclidean distance as

$$\begin{aligned}\mathbf{z}^* &= \arg\min_{\mathbf{z}} \|\tilde{\mathbf{A}}(\omega^*)\mathbf{z} - \tilde{\mathbf{B}}(\omega^*)\|^2 \\ &= \left[\tilde{\mathbf{A}}(\omega^*)^{\mathrm{T}}\tilde{\mathbf{A}}(\omega^*)\right]^{-1}\tilde{\mathbf{A}}(\omega^*)^{\mathrm{T}}\tilde{\mathbf{B}}(\omega^*), \end{aligned} \tag{13}$$

where $\|\cdot\|$ is a Euclidean norm. It is shown that (13) has the same structure as (11). Last, the origins of all paths $\{(x_p, y_p)\}$ can be computed using the parameters $\{\mathbf{z}^*, \omega^*\}$ as illustrated in E1. Averaging these origins gives the estimate of the HV position $\mathbf{p}^* = (x^*, y^*)$ with $x^* = \frac{1}{P}\sum_{p=1}^{P} x_p$ and $y^* = \frac{1}{P}\sum_{p=1}^{P} y_p$.

Remark 3 (Feasibility to LoS Vehicle Sensing): The proposed technique is also feasible to sense a vehicle in LoS since the LoS path is a special case of NLoS path considering that one virtual scatterer is located on the LoS path. The accuracy of LoS vehicle sensing is much better than that of HV sensing because the received signal power of LoS is much larger that of NLoS, providing more accurate AoA/AoD/ToA estimations. The detailed comparison is given in Section VII.

D. EXTENSION TO 3D PROPAGATION

Consider the scenario that propagation paths lie in the 3D Euclidean space instead of the 2D plane previously assumed. As shown in Fig. 4, the main differences are the elevation angles added to the AoAs, AoDs, and HV orientation. Specially, the AoA includes two angles: θ (azimuth) and ϑ (elevation) and AoD consists φ (azimuth) and ψ (elevation). The estimations of AoAs and AoDs in the 3D model can be jointly estimated via various approaches, e.g., MUSIC algorithm for 3D signal detection (see e.g., [37]). The HV orientation also includes two unknowns: ω (azimuth) and ϱ (elevation). The coordinates of HV, denoted by $\mathbf{p} = (x, y, z)^{\mathrm{T}}$, are given as

$$\begin{cases} x = \nu_p \sin(\vartheta_p)\cos(\theta_p) - (d_p - \nu_p)\sin(\psi_p + \varrho)\cos(\varphi_p + \omega), \\ y = \nu_p \sin(\vartheta_p)\sin(\theta_p) - (d_p - \nu_p)\sin(\psi_p + \varrho)\sin(\varphi_p + \omega), \\ z = \nu_p \cos(\vartheta_p) - (d_p - \nu_p)\cos(\psi_p + \varrho), \end{cases}$$

where $\forall p \in \mathcal{P}$.

Similar to E1, the following system of equations is constructed for 3D propagation:

$$\begin{cases} \nu_p \sin(\vartheta_p)\cos(\theta_p) - (d_p - \nu_p)\sin(\psi_p + \varrho)\cos(\varphi_p + \omega) \\ = \nu_1 \sin(\vartheta_1)\cos(\theta_1) - (d_1 - \nu_1)\sin(\psi_1 + \varrho)\cos(\varphi_1 + \omega), \\ \nu_p \sin(\vartheta_p)\sin(\theta_p) - (d_p - \nu_p)\sin(\psi_p + \varrho)\sin(\varphi_p + \omega) \\ = \nu_1 \sin(\vartheta_1)\sin(\theta_1) - (d_1 - \nu_1)\sin(\psi_1 + \varrho)\sin(\varphi_1 + \omega), \\ \nu_p \cos(\vartheta_p) - (d_p - \nu_p)\cos(\psi_p + \varrho) \\ = \nu_1 \cos(\vartheta_1) - (d_1 - \nu_1)\cos(\psi_1 + \varrho), \end{cases} \tag{E3}$$

where $\forall p \in \mathcal{P}$.

It is shown that the number of equations and the number of unknown variables are $3(P-1)$ and $(P+3)$, respectively. For the HV-sensing problem to be solvable, we require $3(P-1) \geq P+3$, which leads to the following proposition.

Proposition 3 (Sensing Feasibility Condition for 3D): Consider the 3D propagation model. To sense the position and orientation of HV provisioned with a single-cluster array, at least three NLoS signal paths are required, i.e., $P \geq 3$.

Compared with 2D propagation, the minimal number of required signal paths is reduced because extra information can be extracted from one additional dimension (i.e., elevation angles information of AoAs, AoDs) of each signal path. A similar methodology described in Sections III-B and III-C can be easily modified for 3D propagation by applying a 2D search based discriminant to find ω and ϱ over $[0, 2\pi]$ and $[0, \pi]$, respectively.

IV. SENSING HIDDEN VEHICLE WITH A MULTI-CLUSTER ARRAY

The preceding section targets the scenario that the HV is provisioned with a single-cluster array, allowing the SV to sense the HV position and orientation. In the concerned HV scenarios, the SV does not know whether the HV exists and has no size information as prior knowledge. It calls for developing a technique to estimate the HV's size together. To this end, this section considers the scenario where a multi-cluster array is deployed at HV so that SV can sense HV's array size (approximating the HV size) in addition to its position and orientation. Sensing techniques are designed separately for two cases, namely *decoupled* and *coupled* HV antenna clusters, in the following sub-sections.

A. CASE 1: DECOUPLED HV ANTENNA CLUSTERS

Consider the case of decoupled HV antenna clusters via transmission of orthogonal waveform sets over different clusters. As a result, the SV is capable of grouping detected paths according to their originating clusters. This simplifies the HV-sensing in the sequel by building on the techniques in the preceding section.

Recall that four HV antenna clusters are located at the vertices of a rectangle with length L and width W that represents the HV shape (see Fig. 5). The vertex locations are represented as $\{\mathbf{p}^{(k)} = (x^{(k)}, y^{(k)})^{\mathrm{T}}\}_{k=1}^{K}$. Different orthogonal

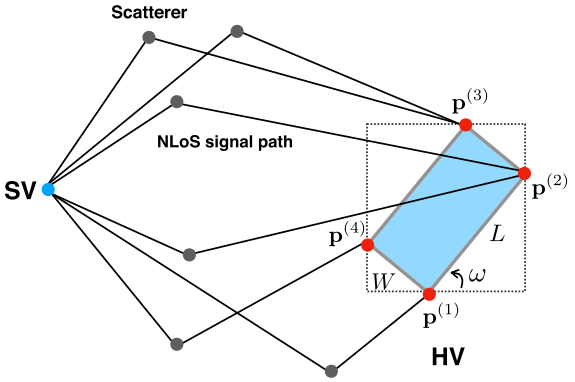

FIGURE 5. Rectangular configuration of a 4-cluster HV array and the corresponding multi-path propagations.

waveform set is assigned to each cluster, allowing SV with prior knowledge on the waveform sets to differentiate the signals transmitted by different clusters. The more challenging case where all clusters are assigned an identical waveform set is studied in the next section. Let each path be ordered based on HV array index such that $\mathcal{P} = \{\mathcal{P}^{(1)}, \mathcal{P}^{(2)}, \mathcal{P}^{(3)}, \mathcal{P}^{(4)}\}$ where $\mathcal{P}^{(k)}$ represents the set of received signals from the k-th HV antenna cluster. Note that the vertices determines the HV size and their centroid that gives the HV position. Therefore, the **sensing problem** can be represented as

$$\bigcup\nolimits_{k=1}^{4} \bigcup\nolimits_{p\in\mathcal{P}^{(k)}} \{\theta_p, \phi_p, \lambda_p\} \Rightarrow \{\{\mathbf{p}^{(k)}\}_{k=1}^{4}, \omega\}. \quad (14)$$

A naive sensing approach is to exploit the orthogonality of multiple waveform sets to decompose the sensing problem into separate positioning of HV antenna clusters using the technique designed in the preceding section. In the following subsection, we propose a more efficient sensing technique exploiting the prior knowledge of the HV clusters' rectangular topology.

1) SENSING FEASIBILITY CONDITION

Without loss of generality, assume that the received signal from the first HV antenna cluster, indexed by the set $\mathcal{P}^{(1)}$, is not empty and $1 \in \mathcal{P}^{(1)}$. Based on the rectangular configuration of $\{\mathbf{p}^{(k)}\}_{k=1}^{4}$ (see Fig. 5), a system of equations is formed:

$$\begin{cases} v_p\cos(\theta_p) - (d_p - v_p)\cos(\varphi_p + \omega) + \eta_p(\omega, L, W) \\ = v_1\cos(\theta_1) - (d_1 - v_1)\cos(\varphi_1 + \omega), \\ v_p\sin(\theta_p) - (d_p - v_p)\sin(\varphi_p + \omega) + \zeta_p(\omega, L, W) \\ = v_1\sin(\theta_1) - (d_1 - v_1)\sin(\varphi_1 + \omega), \end{cases} \quad (E4)$$

where $\eta_p(\omega, L, W) = 0, L\cdot\cos(\omega), L\cdot\cos(\omega) - W\cdot\sin(\omega)$, and $-W\cdot\sin(\omega)$ when $p \in \mathcal{P}^{(1)}, p \in \mathcal{P}^{(2)}, p \in \mathcal{P}^{(3)}$, and $p \in \mathcal{P}^{(4)}$, respectively. $\zeta_p(\omega, L, W)$ is obtained via replacing all cos and sin in $\eta_p(\omega, L, W)$ with sin and $-\cos$, respectively. The number of signal paths is given as $P = |\mathcal{P}| = \sum_{k=1}^{4} |\mathcal{P}^{(k)}|$. Compared with E1, the number of equations in (E4) is the same as $2(P-1)$ while the number of unknowns increases from $(P+2)$ to $(P+4)$ since L and W are also unknown. Consequently, E4 has a unique solution when $2(P-1) \geq P+4$.

Proposition 4 (Sensing Feasibility Condition): Consider the scenario that the HV is provisioned with a 4-cluster array and orthogonal waveform sets are transmitted from different clusters. To sense the position, size, and orientation of the HV, at least six paths are required: $P \geq 6$.

Remark 4 (Advantage of Array-Topology Knowledge): The separate positioning of individual HV antenna clusters requires at least 16 NLoS paths (see Proposition 1). On the other hand, the proposed sensing technique reduces the number of required paths to only 6 by exploiting the prior knowledge of the rectangular configuration of antenna clusters.

2) HIDDEN VEHICLE SENSING

Consider the case where channel noise is negligible. The system of equations in E4 can be rewritten in a compact matrix form:

$$\hat{\mathbf{A}}(\omega)\hat{\mathbf{z}} = \mathbf{B}(\omega), \quad (E5)$$

where $\hat{\mathbf{z}} = (\mathbf{v}, d_1, L, W)^{\mathrm{T}} \in \mathbb{R}^{(P+3)\times 1}$ with $\mathbf{v}$ following the index ordering of $\mathcal{P}$, and $\mathbf{B}(\omega)$ is given in (9). The matrix $\hat{\mathbf{A}}(\omega)$ can be decomposed as

$$\hat{\mathbf{A}}(\omega) = \left[\mathbf{A}(\omega)\ \mathbf{L}(\omega)\ \mathbf{W}(\omega)\right] \in \mathbb{R}^{2(P-1)\times(P+3)}, \quad (15)$$

where $\mathbf{A}(\omega)$ follows (7). Moreover, $\mathbf{L}(\omega) \in \mathbb{R}^{2(P-1)\times 1}$ is given as $[\mathbf{L}^{(\cos)}(\omega), \mathbf{L}^{(\sin)}(\omega)]^{\mathrm{T}}$ with

$$\mathbf{L}^{(\cos)}(\omega) = [\underbrace{0, \cdots, 0}_{|\mathcal{P}^{(1)}|-1}, \underbrace{-\cos(\omega), \cdots, -\cos(\omega)}_{|\mathcal{P}^{(2)}|+|\mathcal{P}^{(3)}|}, \underbrace{0, \cdots, 0}_{|\mathcal{P}^{(4)}|}]^{\mathrm{T}},$$

where $|\mathcal{P}^{(k)}|$ counts the number of elements in $\mathcal{P}^{(k)}$ and $\mathbf{L}^{(\sin)}(\omega)$ is obtained by replacing all $\cos(\omega)$ in $\mathbf{L}^{(\cos)}(\omega)$ with $\sin(\omega)$. $\mathbf{W}(\omega)$ can be written as $[\mathbf{W}^{(\sin)}(\omega), \mathbf{W}^{(\cos)}(\omega)]^{\mathrm{T}}$ where

$$\mathbf{W}^{(\sin)}(\omega) = [\underbrace{0, \cdots, 0}_{|\mathcal{P}^{(1)}|+|\mathcal{P}^{(2)}|-1}, \underbrace{\sin(\omega), \cdots, \sin(\omega)}_{|\mathcal{P}^{(3)}|+|\mathcal{P}^{(4)}|}]^{\mathrm{T}},$$

and $\mathbf{W}^{(\cos)}(\omega)$ is obtained by replacing all sin in $\mathbf{W}^{(\sin)}(\omega)$ with $-\cos$.

1) Computing ω^*: Noting that E5 is over-determined when $P \geq 6$, the resultant discriminant of the orientation ω is similar to that in Proposition 2 and given as follows.

Proposition 5 (Discriminant of Orientation): With $P \geq 6$, the unique ω^* exists when $\hat{\mathbf{B}}(\omega^*)$ is orthogonal to the null column space of $\hat{\mathbf{A}}(\omega^*)$ denoted by $\mathsf{null}(\hat{\mathbf{A}}(\omega^*)^{\mathrm{T}}) \in \mathbb{R}^{2(P-1)\times(P+1)}$:

$$\mathsf{null}(\hat{\mathbf{A}}(\omega^*)^{\mathrm{T}})^{\mathrm{T}}\hat{\mathbf{B}}(\omega^*) = \mathbf{0}. \quad (16)$$

Given this discriminant, a simple 1D search can be performed over the range $[0, 2\pi]$ to find ω^*.

2) Computing $\{\mathbf{p}^{(k)}\}_{k=1}^{4}$: Given the ω^*, E5 can be solved by

$$\hat{\mathbf{z}}^* = \left[\hat{\mathbf{A}}(\omega^*)^{\mathrm{T}}\hat{\mathbf{A}}(\omega^*)\right]^{-1}\hat{\mathbf{A}}(\omega^*)^{\mathrm{T}}\hat{\mathbf{B}}(\omega^*). \quad (17)$$

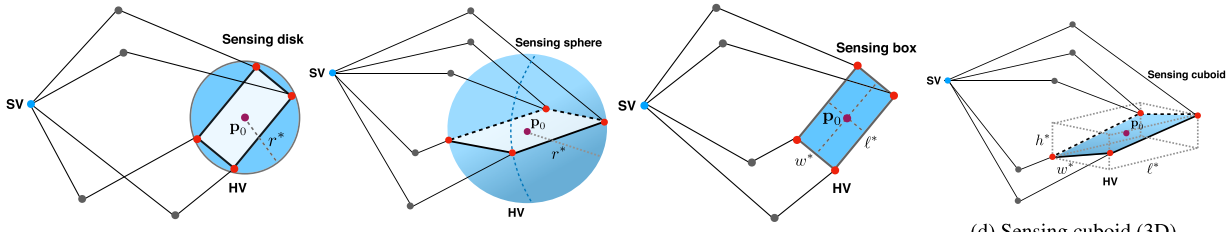

(a) Sensing disk (2D). (b) Sensing sphere (3D). (c) Sensing box (2D). (d) Sensing cuboid (3D).

FIGURE 6. Different approaches of HV-sensing for the scenario of a 4-cluster HV array and an identical waveform set for transmission by different HV antenna clusters.

The positions of HV antenna clusters, say $\{\mathbf{p}^{(k)}\}_{k=1}^4$, can be computed by substituting (16) and (17) into (6) and (E4). Extending the above sensing technique to the case with channel noise is straightforward by modifying (16) to a minimization problem as in Section III-C.

B. CASE 2: COUPLED HV ANTENNA CLUSTERS

It is desired to reduce the number of orthogonal waveform sets used by a HV so as to facilitate multi-access by dense HVs. Thus, in this section, we consider the resource-limited case of coupled HV antenna clusters where an identical waveform set is shared and transmitted by all HV antenna clusters. The design of HV-sensing is more challenging since the SV is incapable of grouping the signal paths according to their originating HV antenna clusters. For tractability, the objectives of HV-sensing for this scenario is redefined as: 1) positioning of the centroid of HV multi-cluster array denoted by $\mathbf{p}_0 = (x_0, y_0)$; 2) sensing the HV size by estimating the maximum distance between HV antenna clusters and $\mathbf{p}_0$, denoted by $R = \max_k |\mathbf{p}^{(k)} - \mathbf{p}_0|$; 3) estimating the HV orientation ω. It follows that the **sensing problem** can be formulated as

$$\bigcup\nolimits_{p\in\mathcal{P}}\{\theta_p, \phi_p, \lambda_p\} \Rightarrow \{\mathbf{p}_0, R, \omega\}. \tag{18}$$

To solve the problem, we adopt the following two-step approach:

Step 1: By assuming that all signals received at SV originate from the same transmitting location, it is treated as the HV array centroid and estimated together with the orientation ω using the technique in Section III.

Step 2: Given ω and $\mathbf{p}_0$, the size parameter R can be estimated by solving optimization problems based on bounding the HV array by either a disk or a box.

The techniques for Step 2 are designed in following sub-sections.

1) HV SIZE SENSING BY DISK MINIMIZATION

Note that the HV array is outer bounded by a disk. Then the problem of estimating the HV size parameter R at SV can be translated into the optimization problem of minimizing the bounding-disk radius. As shown in Fig. 6(a), we define a *sensing disk* $\mathcal{C}(\mathbf{p}_0, r)$ centered at the estimated centroid $\mathbf{p}_0$ with the radius r:

$$\mathcal{C}(\mathbf{p}_0, r) = \left\{(x, y)|\,(x - x_0)^2 + (y - y_0)^2 \le r^2\right\}. \tag{19}$$

A constraint is applied that all HV antennas, or equivalently the origins of all signal paths received at the SV, should lie within the disk. Then estimating the HV size R can be translated into the following problem of *disk minimization*:

$$\begin{aligned} R = \min_{d_1, r, \{v_p, x_p, y_p\}} \; & r \\ \text{s.t. } & \left(x_p - x_0\right)^2 + \left(y_p - y_0\right)^2 \le r^2, \;\; 0 < v_p < d_1 + c\rho_p, \\ & (x_p, y_p) \text{ satisfies (4) with } d_p = d_1 + c\rho_p, \;\; \forall p \in \mathcal{P}, \end{aligned} \tag{E6}$$

where the first constraint is as mentioned above and the second represents the distance after the reflection v_p cannot exceed the total propagation distance d_p represented in terms of d_1 and TDoA ρ_p as $d_p = d_1 + c\rho_p$ with $\{\rho_p\}$ being the TDoAs [see (6)]. The values of $\{x_p, y_p\}$ are directly calculated by plugging the optimized d_1 and $\{v_p\}$ into E1, corresponding to the optimal radius r^* according to the first constraint of E6. One can observe that Problem E6 is a problem of *second-order cone programming* (SOCP). Thus, it is a convex optimization problem and can be efficiently solved numerically e.g., using the efficient MatLab toolbox such as CVX.

Analyzing the problem structure can shed light on the number of required paths for HV-sensing in the current scenario. The existence and uniqueness of the optimal solution r^* for Problem E6 can be explained intuitively by considering the feasible range of d_1. Let $\mathcal{S}_p(r)$ represent the feasible range of the optimization variable d_1 for path p when the disk radius is given as r:

$$\mathcal{S}_p(r) = \{d_1\,|\text{all constraints for path } p \text{ in E6}\}. \tag{20}$$

Then the feasible range of d_1, denoted by $\mathcal{S}(r)$, is the intersection of the feasible range of d_1 for every path p, i.e., $\mathcal{S}(r) = \bigcap_{p\in\mathcal{P}} \mathcal{S}_p(r)$. This is because all the paths share the same d_1 and thus the feasible range of d_1 should satisfy all paths' constraints in E6 simultaneously. Next, it is straightforward to show the following monotonicity of $\mathcal{S}(r)$: $\mathcal{S}(r_1) \subseteq \mathcal{S}(r_2)$ if $r_1 \le r_2$ with $\mathcal{S}(0) = \emptyset$. Based on the monotonicity, there always exists an optimal and unique solution r^* for

Problem E6 such that $\mathcal{S}(r) \neq \emptyset$ if $r \geq r^*$ or otherwise $\mathcal{S}(r) = \emptyset$. In other words,

$$r^* = \inf\{r > 0 \,|\mathcal{S}(r) \neq \emptyset\} = \sup\{r > 0 \,|\mathcal{S}(r) = \emptyset\}.$$

The value r^* corresponds to the critical case where there exist two feasible range sets $\mathcal{S}_p(r^*)$ and $\mathcal{S}_{p'}(r^*)$ only contact each other at their boundaries such that $\mathcal{S}(r)$ contains a single feasible point d_1^* that corresponds to r^*. This leads to the following proposition.

Proposition 6 (HV Size Sensing by Disk Minimization): Given the solution r^* for Problem E6, there always exist at least two paths, say p_1 and p_2, whose originating positions lie on the boundary of the minimized disk $\mathcal{C}(\mathbf{p}_0, r^*)$:

$$\begin{aligned}\left(x_{p_1} - x_0\right)^2 + \left(y_{p_1} - y_0\right)^2 &= \left(x_{p_2} - x_0\right)^2 + \left(y_{p_2} - y_0\right)^2 \\ &= (r^*)^2. \end{aligned} \tag{21}$$

Instead of the earlier intuitive argument, Proposition 6 can be proved rigorously using the *Karush-Kuhn-Tucker* (KKT) conditions as shown in Appendix B.

Remark 5 (Feasible Condition of HV Sensing by Disk Minimization): Though two paths are required to determine the optimal disk radius $R = r^*$ based on Proposition 6, at least four paths are required for estimating the required centroid $\mathbf{p}_0$ (see Proposition 1).

Remark 6 (Extension to 3D Propagation): The extension to 3D propagation model in Section III-D is straightforward by using a sphere instead of a disk [see Fig. 6(b)]. The resultant sphere minimization problem has the same form as Problem E6 except that the first constraint modified as $\left(x_p - x_0\right)^2 + \left(y_p - y_0\right)^2 + \left(z_p - z_0\right)^2 \leq r^2, \ \forall p \in \mathcal{P}$, where the centroid $\mathbf{p}_0 = (x_0, y_0, z_0)$ is estimated using the technique in Section III-D. Again, the problem can be optimally solved since it still follows SOCP structure.

2) HV SIZE SENSING BY BOX MINIMIZATION

In the preceding sub-section, the HV size is estimated by bounding the HV array by a disk and then minimizing it. In this sub-section, the disk is replaced by a box and the HV size estimation is translated into the problem of box minimization. Compared with disk minimization, the current technique improves the estimation accuracy since a vehicle typically has a rectangular shape. Let L and W be the length and width of the rectangular where the HV antenna clusters are placed at its vertices (see Fig. 6(c)). Then the problem of HV size sensing is to estimate both L and W. Recall that the HV array centroid $\mathbf{p}_0$ and orientation ω are estimated in **Step 1** of the proposed sensing approach as mentioned. Given $\mathbf{p}_0$ and ω, we define a *sensing box* for bounding the HV array, denoted as $\mathcal{B}(\mathbf{p}_0, \omega, \ell, w)$, as an ω-rotated rectangle centered at $\mathbf{p}_0 = (x_0, y_0)$ and having the length ℓ and width w:

$$\begin{aligned}\mathcal{B}(\mathbf{p}_0, \omega, \ell, w) = \Bigg\{(x, y) \Bigg| &-\frac{1}{2}\left[\ell, w\right]^{\mathrm{T}} \\ &\preceq \mathbf{R}(\omega)\left[x - x_0, y - y_0\right]^{\mathrm{T}} \preceq \frac{1}{2}\left[\ell, w\right]^{\mathrm{T}}\Bigg\},\end{aligned} \tag{22}$$

where $\mathbf{R}(\omega)$ is the counterclockwise rotation matrix with the rotation angle ω given as

$$\mathbf{R}(\omega) = \begin{bmatrix} \cos(\omega) & \sin(\omega) \\ -\sin(\omega) & \cos(\omega) \end{bmatrix}, \tag{23}$$

and $\preceq$ represents an element-wise inequality. Like disk minimization in the previous subsection, finding the correct L and W is transformed into the following *box minimization* problem:

$$\begin{aligned}\{L, W\} = \arg \min_{d_1, \ell, \omega, \{v_p, x_p, y_p\}} &(\ell^2 + w^2) \\ \text{s.t. } -\frac{1}{2}\left[\ell, w\right]^{\mathrm{T}} &\preceq \mathbf{R}(\omega)\left[x_p - x_0, y_p - y_0\right]^{\mathrm{T}} \\ &\preceq \frac{1}{2}\left[\ell, w\right]^{\mathrm{T}}, \\ 0 < v_p &< d_1 + c\rho_p, \quad \forall p \in \mathcal{P}, \end{aligned} \tag{E7}$$

where the first constraint represents that all origins of signal paths $\{x_p, y_p\}$ should be inside $\mathcal{B}(\mathbf{p}_0, \omega, \ell, w)$ defined in (22) and the second one is the same as in E6. Problem E7 can be solved by *quadratic programming* (QP), which is a convex optimization problem and can be efficiently solved using a software toolbox such as MatLab CVX. A result similar to that in Proposition 6 can be obtained for HV size sensing by box minimization as shown below.

Proposition 7 (HV Size Sensing by Box Minimization): Given the solution $\{\ell^*, w^*\}$ for Problem E7, there always exist at least two paths, say p_1 and p_2, whose originating positions lie on two different vertices of the minimized box:

$$\begin{aligned}&\mathbf{R}(\omega)\left[x_{p_1}^* - x_{p_2}^*, y_{p_1}^* - y_{p_2}^*\right]^{\mathrm{T}} \\ &= \left[\ell^*, w^*\right]^{\mathrm{T}} \text{ or } \left[-\ell^*, w^*\right]^{\mathrm{T}} \text{ or } \left[\ell^*, 0\right]^{\mathrm{T}} \text{ or } \left[0, w^*\right]^{\mathrm{T}}. \end{aligned} \tag{24}$$

Proof: See Appendix C

Remark 7 (Feasible Condition of HV-Sensing by Box Minimization): A similar remark as Remark 5 for disk minimization also applies to the current technique. Specifically, though two paths are required to determine the optimal box length $L = \ell^*$ and width $W = w^*$ based on Proposition 7, at least four paths are required for estimating the required HV centroid $\mathbf{p}_0$ and orientation ω (see Proposition 1).

Remark 8 (Sensing Box Minimization for Decoupled Antenna Clusters): The technique of HV size sensing by box minimization developed for the case of coupled HV antenna clusters can be also modified for use in the case of decoupled clusters. Roughly speaking, the modified technique involves separation minimization of four boxes corresponding to the positioning of four antenna clusters. As the modification is straightforward, the details are omitted for brevity. The resultant advantage with respect to the original sensing technique proposed in Section IV-A is to reduce the minimum number of required paths from 6 (see Proposition 4) to 4.

Remark 9 (Extension to 3D Propagation): Similar to Remark 6 for disk minimization, the technique of HV size sensing by box minimization originally designed for 2D propagation can be extended to 3D propagation model by using a cuboid instead of a box, yielding the problem of

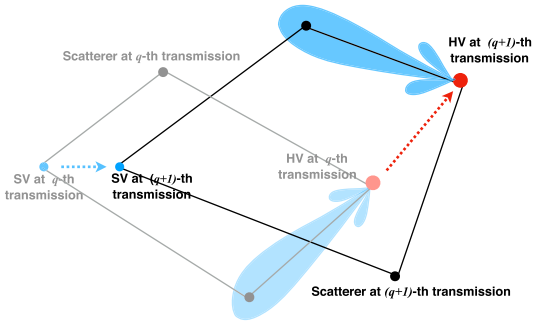

FIGURE 7. Proposed solutions for coping with insufficient number of propagation paths.

cuboid minimization as illustrated in Fig. 6(d). Compared with E7, the objective function of the cuboid minimization is $\ell^2+w^2+h^2$ where the new variable h is added to represent the height of the cuboid. In addition, the first constraint in E7 is modified as

$$-\frac{1}{2}\left[\ell, w, h\right]^{\mathrm{T}} \preceq \mathbf{R}_{3\mathrm{D}}(\omega, \varrho)\left[x_p - x_0, y_p - y_0, z_p - z_0\right]^{\mathrm{T}} \preceq \tfrac{1}{2}\left[\ell, w, h\right]^{\mathrm{T}}, \quad \forall p \in \mathcal{P} \tag{25}$$

where $\mathbf{R}_{3\mathrm{D}}(\omega, \varrho)$ is the 3D counterclockwise rotation matrix with the rotation angles ω and ϱ as

$$\mathbf{R}_{3\mathrm{D}}(\omega, \varrho) = \begin{bmatrix} \cos(\omega) & -\sin(\omega)\cos(\varrho) & \sin(\omega)\sin(\varrho) \\ \sin(\omega) & \cos(\omega)\cos(\varrho) & -\cos(\omega)\sin(\varrho) \\ 0 & \sin(\varrho) & \cos(\varrho) \end{bmatrix}, \tag{26}$$

and the centroid $\mathbf{p}_0 = (x_0, y_0, z_0)$ can be obtained by the technique in Section III-D. The cuboid minimization is still QP and the solution approach is similar to that for the 2D counterpart.

V. COPING WITH INSUFFICIENT MULTI-PATH

The HV-sensing techniques designed in the preceding sections require at least four propagation paths to be effective. In practice, it is possible to happen that the number of observed (i.e., detectable) paths may be insufficient, i.e., $P < 4$, due to either sparse scatterers or the fact that most paths are severely attenuated. To address this practical issue, two solutions are proposed in the following sub-sections, called *sequential path combining* and *random directional beamforming*. For simplicity, we focus on the case of single-cluster HV array while the extension to the case of multi-cluster array is straightforward.

A. SEQUENTIAL PATH COMBINING

As shown in Fig. 7, the technique of sequential path combining implemented at the SV merges paths from repeated transmissions of HV till a sufficient number of paths is identified for the purpose of subsequent HV-sensing. Let Q denote the number of HV's repetitive transmissions with a constant interval denoted by Δ. The interval is chosen to be much larger than the coherence time, enabling SV to differentiate the arrival paths according to their transmission time instants. In addition, the total transmission duration $Q\Delta$ should be sufficiently small enough to guarantee the constant velocities of HV and SV within the duration. Assume that the relative orientation of driving direction and velocity of HV with respect to SV, namely ω and v, remain constant within the entire duration of Q intervals $Q\Delta$. Let $\mathcal{P}_q$ denote the set of observed paths of the q-th transmission. Then the following system of equations are formed:

$$\begin{cases} \nu_p \cos(\theta_p) - (d_p - \nu_p)\cos(\varphi_p + \omega) + v(q-1)\cos(\omega) \\ = \nu_1 \cos(\theta_1) - (d_1 - \nu_1)\cos(\varphi_1 + \omega), \\ \nu_p \sin(\theta_p) - (d_p - \nu_p)\sin(\varphi_p + \omega) + v(q-1)\sin(\omega) \\ = \nu_1 \sin(\theta_1) - (d_1 - \nu_1)\sin(\varphi_1 + \omega). \end{cases}$$

where $p \in \mathcal{P}_q$ and $q = 1, 2, \cdots, Q$. They can be solved following a similar procedure as in Section IV-A. Let $P_{1:q}$ be the total number of paths identified due to the q transmissions, i.e., $P_{1:q} = |\mathcal{P}_1| + |\mathcal{P}_2| + \cdots + |\mathcal{P}_q|$. Noting that the number of equations above is $2(P_{1:q} - 1)$ and the number of unknowns are $(P_{1:q} + 3)$ including $\{\nu_p\}$, d_1, ω and v. As a result, the condition for the SV collecting sufficient paths for HV sensing is $2(P_{1:q} - 1) \leq (P_{1:q} + 3)$ or equivalently $P_{1:q} \geq 5$. So path combining over multiple sequential transmissions overcomes the practical limitation of insufficient paths.

B. RANDOM DIRECTIONAL BEAMFORMING

To further enhance the effectiveness of sequential path combining, a directional beam can be randomly steered at HV over sequential transmissions. Its purpose is to reveal some paths that are otherwise hidden to SV due to severe attenuation. The beam width can be set as ranging from 90° to 30° with gain ranging from 3 dB to 10 dB, which helps reach faraway scatterers by focusing the transmission power in their directions and thereby mitigating path loss [38]. Note that a single trial of randomly steered beam may not find enough paths. Thus, it is important to combine the technique with sequential path combining designed in the preceding subsection for the former to be effective. Their integrated operation is illustrated in Fig. 7 and its effectiveness is verified by simulation in the sequel.

VI. EXTENSION TO MULTI-VEHICLE VEHICULAR POSITIONING

The current two-vehicle based positioning scenarios can be extended to multi-vehicle scenario straightforwardly by jointly using the following two approaches.

- *Waveform Pool & Sensing*: Interference-free multi-vehicle sensing is possible if multiple orthogonal waveforms are given, called a *waveform pool*. The list of waveforms in the pool is periodically broadcast by a *road side unit* (RSU), and each vehicle knows the list. Before selecting a waveform, the usages of all waveforms in the list are sensed. It is analogy to a carrier sensing mechanism in WiFi communication, and it is thus called a *waveform sensing*. To avoid waveform

TABLE 2. Simulation settings.

Simulation parameter	Value
Carrier frequency f_c, transmission bandwidth B	5.9 GHz, 100 MHz
Number of transmit, receive antennas per cluster $\{M_t, M_r\}$	$\{20, 20\}$
Transmit power, noise power	23 dBm, -70 dBm
Size of vehicle $L \times W$, inter-vehicle distance	3×6 m^2, 50 m
Relative velocity between HV and SV v (driving in opposite directions)	200 km/h

collision, one waveform is selected in the list except the ones being used by nearby vehicles.

- *Geo-Zoning*: In spite of using waveform sensing, more than two vehicles could select the same waveform simultaneously if they are out of their sensing coverage, named as *hidden vehicle problem* (HVP). To avoid HVP, a spatial isolation should be created where vehicles in different locations would be limited to select the resources for transmission from a certain time-frequency set, based on their absolute geographical location. In 3GPP specification, it is called geo-zoning or zone-based resource allocation [39].

VII. SIMULATION RESULTS

In this section, the performance of the proposed vehicular sensing techniques are evaluated by realistic simulation. Consider the V2V channel model. We adopt the geometry-based stochastic channel model given in [31] for modeling the practical scatterers distribution and V2V propagation channel, which has been validated by real measurement data. Two types of scatterers, namely mobile scatterers (e.g., from moving vehicles) and static scatterers (e.g., from road signs and buildings), are simulated. As illustrated in Fig. 8(a), in the highway scenario, most of the scatterers are mobile scatterers. On the other hand, in the rural scenario illustrated in Fig. 8(b), the scatterers include vehicles on the road as well as relatively denser stationary objects off the road. The locations of mobile and static scatterers are randomly distributed over the entire area depending on their densities described in [31, Table 1]. Given the scatterer location, the corresponding AoA and AoD are determined without explicit distribution. If more than two scatterer locations are close to each other, the corresponding paths are unresolvable due to similar AoAs and AoDs. Instead, they are observed as a single signal path with higher power. We set the relative velocity and the resultant Doppler shift as zero unless specified since its effects on positioning accuracy are separately verified in Fig. 14. The key simulation parameters and their values are summarized in Table 2 unless stated otherwise. We use MatLab and its CVX tool box for solving optimization problems and simulations.

A. VEHICULAR POSITIONING

The metric for measuring positioning accuracy is defined as the average Euclidean squared distance of estimated positions of vehicle antenna clusters to their true locations: $\frac{1}{4}\sum_{k=1}^{4} \|\mathbf{p}^{*(k)} - \mathbf{p}^{(k)}\|^2$, named *average positioning error*. Note that the metric also indirectly measures the accuracy of

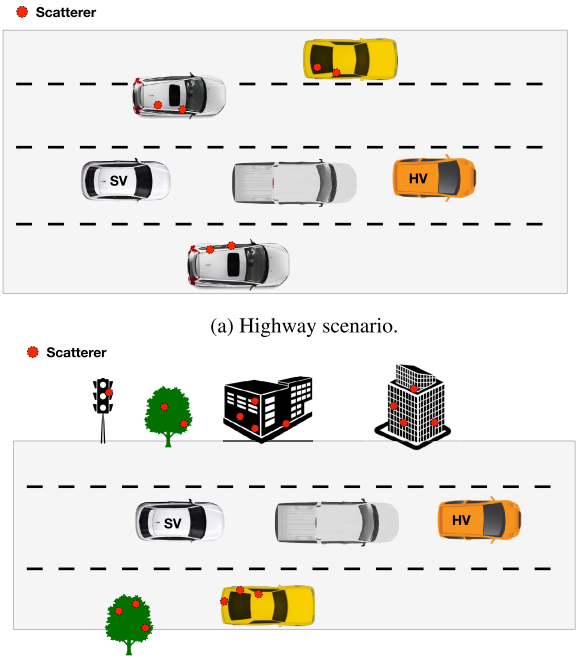

(a) Highway scenario.

(b) Rural scenario.

FIGURE 8. Two typical driving scenarios considered in simulation.

estimated vehicle size and orientation that are determined by the clusters positions.

Fig. 9 shows the performance of the proposed vehicular sensing techniques in the 2D propagation model. The curves of average positioning error versus varying number of observed signal paths and inter-vehicle distance are plotted in Fig. 9(a) and 9(b), respectively. For the case of decoupled antenna clusters using different orthogonal waveform sets, the LS estimator given in Section IV-A is applied, which is feasible if $P \geq 6$ (see Proposition 4). On the other hand, for the case of coupled clusters, the technique of sensing box minimization in Section IV-B.2 is used requiring the number of observed paths $P \geq 4$. Several key observations can be made as follows. First, from Fig. 9(a), receiving more observed paths at SV can dramatically decrease the positioning error and the positioning accuracy is significantly higher in the case of decoupled clusters than the other case. Second, the positioning accuracy in the rural scenario is better than that in the highway scenario due to the following two reasons: 1) the signal propagation loss in the highway scenario is higher than that in the rural counterpart as typically longer distance between vehicles and scatterers adds to the difficulty of accurate sensing; 2) more paths exist in the rural scenario due to denser scatterers, which help improve the positioning accuracy.

Next, in Fig. 9(b), it is shown that the average positioning error increases as the inter-vehicle distance grows because larger path loss degrades sensing performance. The gap of positioning error between the highway and rural scenarios increases with the inter-vehicle distance as the path loss scales up faster in the former than the latter.

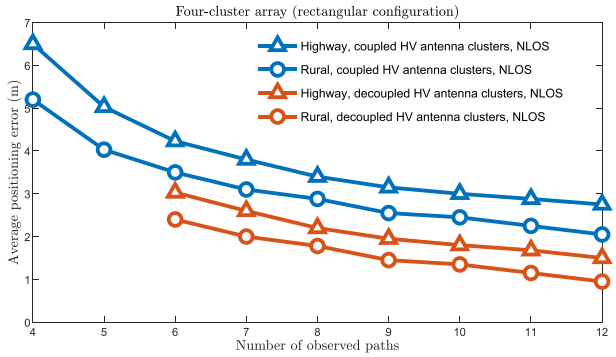

(a) Effect of number of observed signal paths.

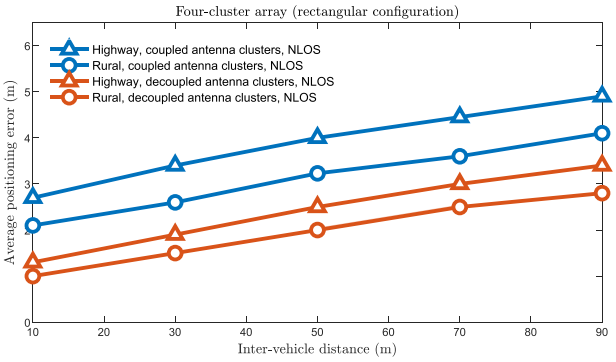

(b) Effect of inter-vehicle distance.

FIGURE 9. Vehicular sensing accuracy under different number of signal paths and the inter-vehicle distance.

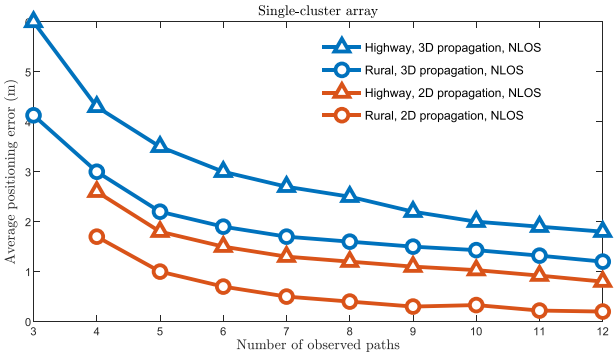

(a) Effect of number of observed signal paths.

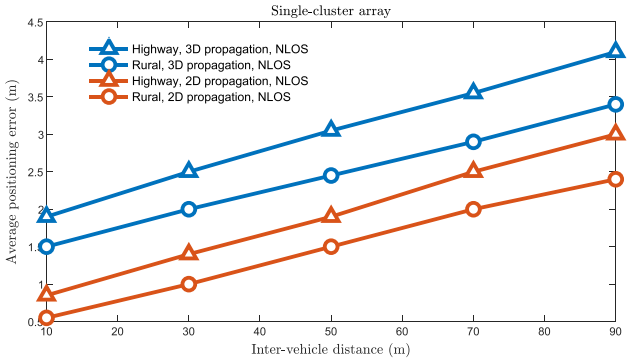

(b) Effect of inter-vehicle distance.

FIGURE 10. Comparison of positioning accuracy between 2D and 3D propagations.

B. COMPARISON BETWEEN 2D AND 3D PROPAGATIONS

Average positioning errors for 2D and 3D propagations are compared in Fig. 10 for varying number of signal paths and inter-vehicle distance. We simulate the case that vehicle uses single-cluster array for transmission. First of all, the main trends shown in Fig. 10 are same as plotted in Fig. 9. Specifically, according to Fig. 10(a), the positioning for 2D and 3D propagation are feasible when $P \geq 4$ and $P \geq 3$, respectively, aligned with Propositions 1 and 3, respectively. Next, it is observed from both Fig. 10(a) and (b) that, compared with 2D propagation, the positioning accuracy for the 3D case is worse and the error gap between the highway and rural scenarios becomes larger. Due to relatively low scatterer height compared with the inter-vehicle distance, most elevation angles are around $\frac{\pi}{2}$, and the resultant positioning accuracy tends to be sensitive to noisy angle detection. In addition, angle detection for 3D propagation is less accurate on the highway due to the larger propagation loss.

C. VEHICULAR SIZE SENSING

In the preceding results, we assume decoupled antenna clusters by using multiple orthogonal waveform sets for transmission. Next, we consider the case of coupled clusters and evaluate the performance of the vehicle size sensing techniques developed in Section IV-B. To this end, we define a *sizing error* as the area difference between the estimated size [sensing disk in (19) or sensing box in (22)] and the real one. Fig. 11 plots the average sizing errors of the disk and box minimizations versus the inter-vehicle distance. Box minimization provides better sizing performance by exploiting the antenna clusters array configuration that is neglected by disk minimization.

Besides, we deploy more antennas per cluster or using larger transmission bandwidth to further improve the size sensing accuracy. It is observed in Fig. 11(a) that the average sizing errors can be reduced by $1.5-3$ (m) for NLoS case and $1-2$ (m) for LoS case, respectively, by deploying 10 more antennas per cluster. In Fig. 11(b), it is shown that the average sizing errors can be reduced by $1.2-2$ (m) for NLoS case and $1-2$ (m) for LoS case, respectively, by using 50 MHz transmission bandwidth more.

D. THE EFFECTS OF A LoS PATH, TRANSMISSION POWER, AND RELATIVE VELOCITY

Fig. 12 verifies the feasibility of the proposed technique for sensing a vehicle in the LoS condition. It is shown that the LoS path contributes to reducing positioning errors in both 2D and 3D propagation models due to its stronger signal strength than other NLoS paths, leading to more accurate TDoA/AoA/AoD detections as mentioned in Remark 3.

As observed in the graphs so far, the positioning accuracy is improved when the number of observed signal paths increases, which can be achieved by using higher

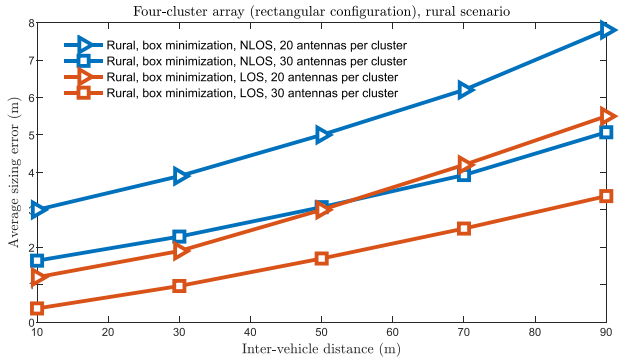

(a) Effect of number of antennas per cluster on sizing accuracy.

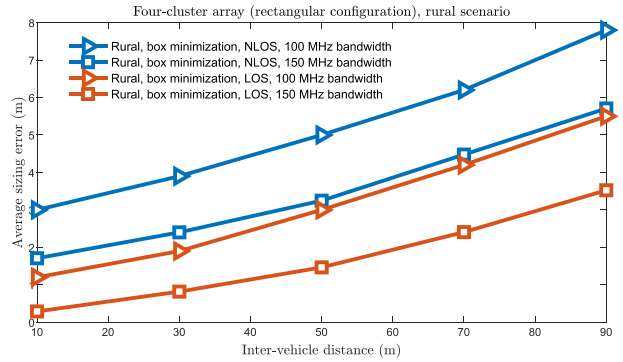

(b) Effect of transmission bandwidth on sizing accuracy.

FIGURE 11. Effect of inter-vehicle distance on average sizing accuracy.

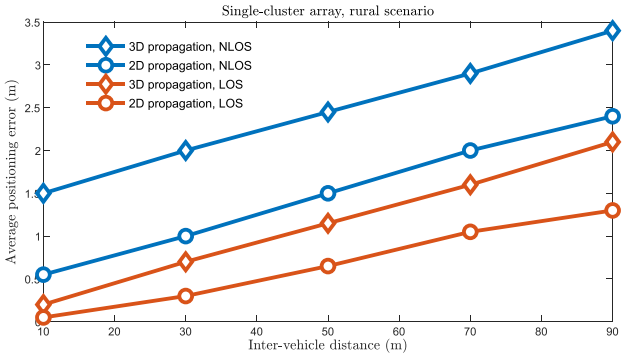

FIGURE 12. Comparison of positioning accuracy between the cases with and without LoS path.

transmission power. Fig. 13 validates its effect on positioning accuracy. It is shown that the positioning error can be reduced with higher transmission power because it helps the SV to detect more signal paths.

Fig. 14 shows the effect of HV-SV relative velocity on positioning accuracy. A more significant Doppler shift due to higher relative speed causes frequent variations of channel parameters such as AoA, AoD, and ToA. Therefore, the perfect orthogonality of the transmitted waveforms is not perfectly guaranteed, which results in the degradation of positioning accuracy. Nevertheless, it is shown that the degeneration is marginal with the practical range of velocity [less than 200 (km/h)].

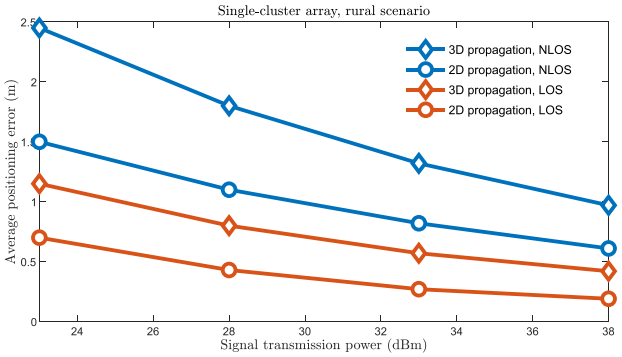

FIGURE 13. Effect of signal transmission power on positioning accuracy.

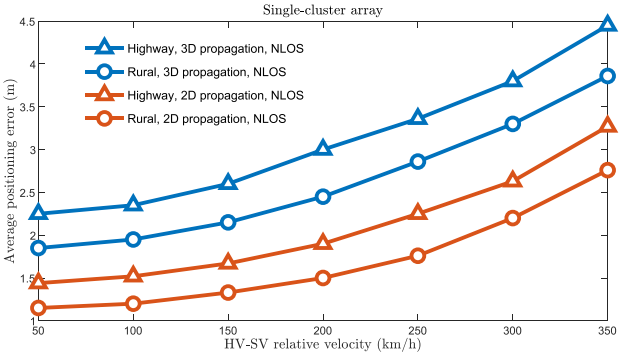

FIGURE 14. Effect of HV-SV relative velocity on positioning accuracy.

E. COPING WITH INSUFFICIENT MULTI-PATH

We evaluate the performance of the integrated solutions of sequential path combining and random directional beamforming both proposed in Section V in the case where scatterers are sparse and there are insufficient paths for vehicular sensing. The vehicle is equipped with a single cluster antenna array and transmits Q repetitive signals with the transmission interval $\Delta = 0.2$ (sec). The setting of Δ satisfies the two requirements explained in Sec. V-A, when considering the maximum coverage of V2V transmission 1 km and assuming that the vehicle's velocity is not changed within 2 seconds. We consider the random beamforming with the beamwidth $\frac{2\pi}{Q}$ and Q time instants sequential combining with $Q = \{1, 2, 4, 8\}$. Note that $Q = 1$ corresponds to isotropic transmission and serves as the benchmark. The metric of *success sensing probability* is defined as the probability that the feasible condition of positioning is satisfied after applying sequential path combining and random directional beamforming. For example, in the case of isotropic transmission, at least 4 paths should be detected at each time instant. On the other hand, in case of random beamforming with sequential path combining, sensing is feasible when the aggregate number of paths over Q time instants should be larger than 5 (see Section V-A). In Fig. 15(a), it is observed that the sensing success probability increases and approaches to one as Q increases. Moreover, Fig. 15(b) shows that the positioning accuracy is improved as sharper beam is used (Q increases) since the angle detections become more accurate.

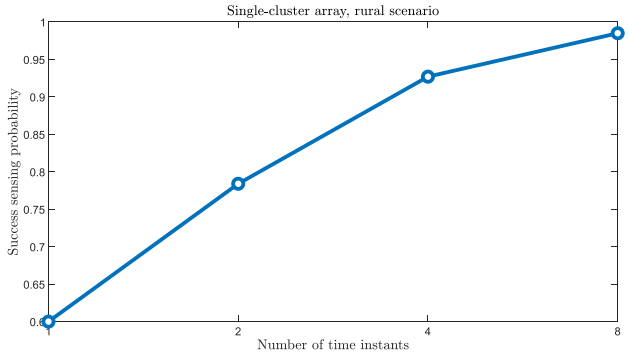

(a) Sensing success probability.

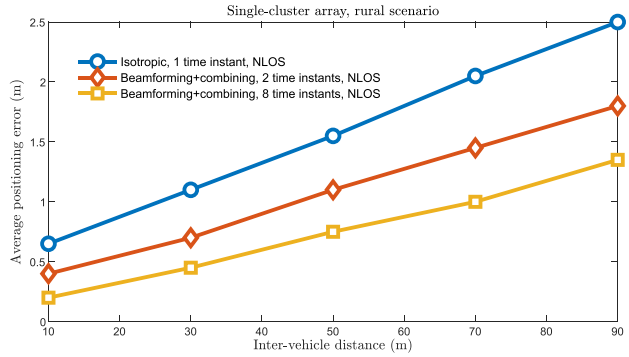

(b) Effect of the inter-distance distance.

FIGURE 15. Coping with insufficient multi-path by sequential path combining and random directional beamforming.

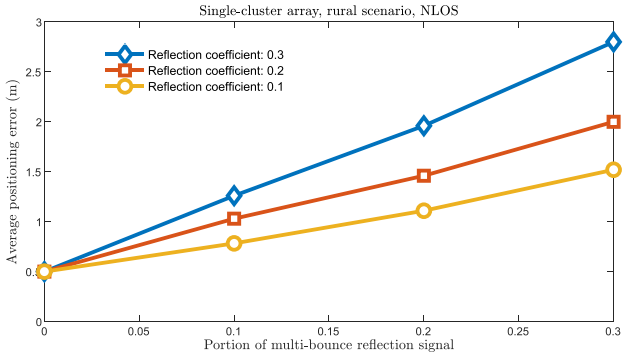

(a) Effect of portion of multi-bounce signal path.

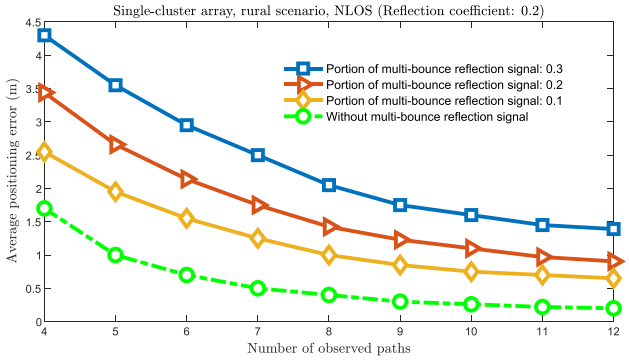

(b) Effect of reflection coefficient.

FIGURE 16. Effects of the multi-bounce scattering on the positioning accuracy under different reflection coefficients.

F. MULTI-BOUNCE SCATTERING

Recall that our positioning technology is developed under the assumption of single-bounce scattering (see Assumption 1). In rich scattering scenarios, however, signals are likely to reflect more than two bounces, defined as multi-bounce scattering, which results in the degradation of the positioning accuracy because the triangular geometry introduced in Section II-A is not satisfied any more. To investigate this effect, we consider an additional simulation scenario where single-bounce and multi-bounce scattering coexist. The multi-bounce signal paths are more attenuated than single-bounce paths by multiplying the receive power with an additional reflection coefficient. Fig. 16(a) presents the positioning error with respect to the fraction of multi-bounce signal paths, showing that the performance degradation is reduced as the additional reflection coefficient reduces. The reason is that multi-bounce paths usually have insufficient signal strengths, making the SV difficult to observe them. As a result, the dominant observed paths are single-bounce signals from which the AoA, AoD, and ToA are accurately estimated, yielding the acceptable positioning performance with marginal degradation. Fig. 16(b) shows that the positioning error can be significantly decreased when more number of paths are observed. For instant, in case with the reflection loss of multi-bounce signals being 0.1, the positioning error is less than 0.6 (m) when 12 paths are observed.

VIII. CONCLUDING REMARKS

This work presents the technologies for sensing a HV, namely its position, orientation, and size by relying on V2V transmission and exploiting multi-path-geometry. Different techniques have been designed to support tradeoffs between the sensing accuracy and varying practical requirements in terms of bandwidth, signaling complexity, and array configuration. We have also addressed practical issue of insufficient multi-path for HV-sensing via developing effective techniques exploiting path randomness in time domain. The proposed technique can be used to assist the current vehicular sensing technologies via giving the vehicle capability to sense HVs. This work opens a new area of HV-sensing and points to many promising research topics on advanced HV-sensing such as velocity detection by estimating Doppler frequencies and simultaneous sensing of multiple HVs.

APPENDIX

A. PROOF OF PROPOSITION 2

The system of linear equations in E2 has a unique solution if and only if both ranks of its coefficient matrix $\mathbf{A}(\omega)$ and its augmented matrix $[\mathbf{A}(\omega)|\mathbf{B}(\omega)]$ are equal to $(P+1)$, according to Rouché-Capelli theorem (see pp. $56-57$ of [33]). When $P \geq 4$, $\mathbf{A}(\omega)$ becomes a tall matrix, namely, $2(P-1) > P+1$. Since every column of $\mathbf{A}(\omega)$ is independent, it is thus straightforwardly shown that $\mathsf{rank}(\mathbf{A}(\omega))$ is $(P+1)$. Next, noting that the number of columns in the augmented matrix $[\mathbf{A}(\omega)|\mathbf{B}(\omega)]$ is $(P+2)$, $\mathsf{rank}([\mathbf{A}(\omega)|\mathbf{B}(\omega)])$ with an arbitrary ω is $(P+2)$

unless $\mathbf{B}(\omega)$ should be in the subspace of $\mathbf{A}^{\mathrm{T}}(\omega)$. Therefore, $\mathbf{B}(\omega^*)$ should be orthogonal to $\mathsf{null}(\mathbf{A}^{\mathrm{T}}(\omega^*))$. We complete the proof.

B. PROOF OF PROPOSITION 6

The KKT conditions of Problem E6 provide the following equality of the optimal solution as

$$\sum_{p\in\mathcal{P}} \gamma_p \left(2\left(x_p - x_0\right) \frac{\partial x_p}{\partial d_1} + 2\left(y_p - y_0\right) \frac{\partial y_p}{\partial d_1} \right) = 0, \tag{27}$$

$$\gamma_p \left(2\left(x_p - x_0\right) \frac{\partial x_p}{\partial v_p} + 2\left(y_p - y_0\right) \frac{\partial y_p}{\partial v_p} \right) = 0, \quad \forall p \in \mathcal{P}, \tag{28}$$

$$\gamma_p \left(\left(x_p - x_0\right)^2 + \left(y_p - y_0\right)^2 - r^2 \right) = 0, \quad \forall p \in \mathcal{P}, \tag{29}$$

where $\{\gamma_p\}$ represent the Lagrangian multipliers of the first constraint in Problem E6. It is worth noting that at least two γ_p should be strictly positive to satisfy (27) and (28). From (29), it is obvious to lead (21), completing the proof.

C. PROOF OF PROPOSITION 7

The KKT conditions of Problem E7 provide the following equality of the optimal solution as

$$\sum_{p\in\mathcal{P}} \left[\bar{\gamma}_p \left(\cos(\omega) \frac{\partial x_p}{\partial d_1} + \sin(\omega) \frac{\partial x_p}{\partial d_1} \right) + \bar{\mu}_p \left(-\sin(\omega) \frac{\partial x_p}{\partial d_1} + \cos(\omega) \frac{\partial x_p}{\partial d_1} \right) \right] = 0, \tag{30}$$

$$\bar{\gamma}_p \left(\cos(\omega) \frac{\partial x_p}{\partial v_p} + \sin(\omega) \frac{\partial x_p}{\partial v_p} \right) + \bar{\mu}_p \left(-\sin(\omega) \frac{\partial x_p}{\partial v_p} + \cos(\omega) \frac{\partial x_p}{\partial v_p} \right) = 0, \tag{31}$$

where $\bar{\gamma}_p = \gamma_p^{(+)} - \gamma_p^{(-)}$ and $\bar{\mu}_p = \mu_p^{(+)} - \mu_p^{(-)}$ with Lagrangian multipliers of the first constraint represented by $\gamma_p^{(+)}$, $\gamma_p^{(-)}$, $\mu_p^{(+)}$ and $\mu_p^{(-)}$, which are positive only when the corresponding equalities are satisfied. In other words, either $\gamma_p^{(+)}$ $\left(\mu_p^{(+)}\right)$ or $\gamma_p^{(-)}$ $\left(\mu_p^{(-)}\right)$ should be zero.

Some observations are made. First, to satisfy (30) and (31) simultaneously, at least two origins should be located in the boundary. Next, it is shown in (31) such that if $\bar{\gamma}_p \neq 0$ then its counterpart multiplier $\bar{\mu}_p \neq 0$, which implies that the origin located in the boundary should be on the vertex. Last, the origin located at the vertex is equivalent to (24), completing the proof.

ACKNOWLEDGMENT

This article was presented in part at the IEEE VTC 2018-Fall [1].

REFERENCES

[1] K. Han, S.-W. Ko, H. Chae, B.-H. Kim, and K. Huang, "Sensing hidden vehicles by exploiting multi-path V2V transmission," in *Proc. IEEE VTC-Fall*, Chicago, IL, USA, Aug. 2017, pp. 1–5.

[2] J. Choi, V. Va, N. G.-Prelcic, R. Daniels, C. R. Bhat, and R. W. Heath, Jr., "Millimeter-wave vehicular communication to support massive automotive sensing," *IEEE Commun. Mag.*, vol. 54, no. 12, pp. 160–167, Dec. 2016.

[3] X. Cui, T. A. Gulliver, J. Li, and H. Zhang, "Vehicle positioning using 5G millimeter-wave systems," *IEEE Access*, vol. 4, pp. 6964–6973, 2016.

[4] *V2X-Locate Positioning System*, Cohda Wireless, Wayville, SA, Australia, 2016.

[5] L. Balico, A. Loureiro, E. Nakamura, R. Barreto, R. Pazzi, and H. Oliveira, "Localization prediction in vehicular ad hoc networks," *IEEE Commun. Surveys Tuts.*, vol. 20, no. 4, pp. 2784–2803, 4th Quart., 2018.

[6] Q. Li, L. Chen, M. Li, S.-L. Shaw, and A. Nuchter, "A sensor-fusion drivable-region and lane-detection system for autonomous vehicle navigation in challenging road scenarios," *IEEE Trans. Veh. Technol.*, vol. 63, no. 2, pp. 540–555, Feb. 2014.

[7] J. Funke, M. Brown, S. M. Erlien, and J. C. Gerdes, "Collision avoidance and stabilization for autonomous vehicles in emergency scenarios," *IEEE Trans. Control Syst. Technol.*, vol. 25, no. 4, pp. 1204–1216, Jul. 2017.

[8] Y. Cao, T. Jiang, O. Kaiwartya, H. Sun, H. Zhou, and R. Wang, "Toward pre-empted EV charging recommendation through V2V-based reservation system," *IEEE Trans. Syst., Man, Cybern. Syst.*, to be published.

[9] J. Yao, A. T. Balaei, M. Hassan, N. Alam, and A. G. Dempster, "Improving cooperative positioning for vehicular networks," *IEEE Trans. Veh. Technol.*, vol. 60, no. 6, pp. 2810–2823, Jul. 2011.

[10] J. B. Kenney, "Dedicated short-range communications (DSRC) standards in the United States," *Proc. IEEE*, vol. 99, no. 7, pp. 1162–1182, Jul. 2011.

[11] M. Motro, A. Chu, J. Choi, P. Lavieri, A. Pinjari, C. Bhat, J. Ghosh, and R. W. Heath, Jr., "Vehicular ad-hoc network simulations of overtaking maneuvers on two-lane rural highways," *Transp. Res. C, Emerg. Technol.*, vol. 72, pp. 60–76, Nov. 2016.

[12] H. Seo, K.-D. Lee, S. Yasukawa, Y. Peng, and P. Sartori, "LTE evolution for vehicle-to-everything services," *IEEE Commun. Mag.*, vol. 54, no. 6, pp. 22–28, Jun. 2016.

[13] R. W. Heath, Jr., N. González-Prelcic, S. Rangan, W. Roh, and A. M. Sayeed, "An overview of signal processing techniques for millimeter wave MIMO systems," *IEEE J. Sel. Topics Signal Process.*, vol. 10, no. 3, pp. 436–453, Apr. 2016.

[14] C. Perfecto, J. Del Ser, and M. Bennis, "Millimeter-wave V2V communications: Distributed association and beam alignment," *IEEE J. Sel. Areas Commun.*, vol. 35, no. 9, pp. 2148–2162, Jun. 2017.

[15] N. González-Prelcic, R. Méndez-Rial, and R. W. Heath, Jr., "Radar aided beam alignment in mmwave V2I communications supporting antenna diversity," in *Proc. Inf. Theory Appl.*, Jan./Feb. 2016, pp. 1–7.

[16] V. Va, J. Choi, T. Shimizu, G. Bansal, and R. W. Heath, Jr., "Inverse multipath fingerprinting for millimeter wave V2I beam alignment," *IEEE Trans. Veh. Technol.*, vol. 67, no. 5, pp. 4042–4058, May 2018.

[17] H. Zhou, S. Xu, D. Ren, C. Huang, and H. Zhang, "Analysis of event-driven warning message propagation in vehicular ad hoc networks," *Ad Hoc Netw.*, vol. 55, pp. 87–96, Feb. 2017.

[18] B. Schwarz, "LIDAR: Mapping the world in 3D," *Nature Photon.*, vol. 4, no. 7, pp. 429–430, 2010.

[19] R. C. Daniels, E. R. Yeh, and R. W. Heath, Jr., "Forward collision vehicular radar with IEEE 802.11: Feasibility demonstration through measurements," *IEEE Trans. Veh. Technol.*, vol. 67, no. 2, pp. 1404–1416, Feb. 2018.

[20] W. Menzel and A. Moebius, "Antenna concepts for millimeter-wave automotive radar sensors," *Proc. IEEE*, vol. 100, no. 7, pp. 2372–2379, Jul. 2012.

[21] L. Kong, M. K. Khan, F. Wu, G. Chen, and P. Zeng, "Millimeter-wave wireless communications for IoT-cloud supported autonomous vehicles: Overview, design, and challenges," *IEEE Commun. Mag.*, vol. 55, no. 1, pp. 62–68, Jan. 2017.

[22] S. Kuutti, S. Fallah, K. Katsaros, M. Dianati, F. Mccullough, and A. Mouzakitis, "A survey of the state-of-the-art localization techniques and their potentials for autonomous vehicle applications," *IEEE Internet Things J.*, vol. 5, no. 2, pp. 829–846, Apr. 2018.

[23] H. Miao, K. Yu, and M. Juntti, "Positioning for NLOS propagation: Algorithm derivations and Cramer–Rao Bounds," *IEEE Trans. Veh. Tech.*, vol. 56, no. 5, pp. 2568–2580, Sep. 2007.

[24] I. Guvenc and C.-C. Chong, "A survey on TOA based wireless localization and NLOS mitigation techniques," *IEEE Commun. Surveys Tuts.*, vol. 11, no. 3, pp. 107–124, Aug. 2009.

[25] R. Feger, C. Pfeffer, W. Scheiblhofer, C. M. Schmid, M. J. Lang, and A. Stelzer, "A 77-GHz cooperative radar system based on multi-channel FMCW stations for local positioning applications," *IEEE Trans. Microw. Theory Techn.*, vol. 61, no. 1, pp. 676–684, Jan. 2013.

[26] H. Liu, H. Darabi, P. Banerjee, and J. Liu, "Survey of wireless indoor positioning techniques and systems," *IEEE Trans. Syst., Man, Cybern. C, Appl. Rev.*, vol. 37, no. 6, pp. 1067–1080, Nov. 2007.
[27] C. K. Seow and S. Y. Tan, "Non-line-of-sight localization in multipath environments," *IEEE Trans. Mobile Comput.*, vol. 7, no. 5, pp. 647–660, May 2008.
[28] X. Wei, N. Palleit, and T. Weber, "AOD/AOA/TOA-based 3D positioning in NLOS multipath environments," in *Proc. IEEE PIMRC*, Sep. 2011, pp. 1289–1293.
[29] B. Shikur and T. Weber, "TDOA/AOD/AOA localization in nlos environments," in *Proc. IEEE ICASSP*, May 2014, pp. 6518–6522.
[30] *Evolved universal Terrestrial Radio Access (E-UTRA); Requirements for Support of Radio Resource Management*, document 3GPP TR R36.133, Apr. 2019. [Online]. Available: http://www.3gpp.org/
[31] J. Karedal, F. Tufvesson, N. Czink, A. Paier, C. Dumard, T. Zemen, C. F. Mecklenbrauker, and A. F. Molisch, "A geometry-based stochastic MIMO model for vehicle-to-vehicle communications," *IEEE Trans. Wireless Commun.*, vol. 8, no. 7, pp. 3646–3657, Jul. 2009.
[32] K. Yu and Y. J. Guo, "Statistical NLOS identification based on AOA, TOA, and signal strength," *IEEE Trans. Veh. Technol.*, vol. 58, no. 1, pp. 274–286, Jan. 2009.
[33] Z. Ding, Y. Liu, J. Choi, Q. Sun, M. Elkashlan, C.-L. I, and H. V. Poor, "Application of non-orthogonal multiple access in LTE and 5G networks," *IEEE Commun. Mag.*, vol. 55, no. 2, pp. 185–191, Feb. 2017.
[34] M. Rossi, A. M. Haimovich, and Y. C. Eldar, "Spatial compressive sensing for MIMO radar," *IEEE Trans. Signal Process.*, vol. 62, no. 2, pp. 419–430, Jan. 2014.
[35] M. Flament, *Path Towards 5G for the Automotive Sector*, 5G Automotive Association, 3GPP, Oct. 2018.
[36] M. K. Ozdemir and H. Arslan, "Channel estimation for wireless OFDM systems," *IEEE Commun. Surveys Tuts.*, vol. 9, no. 2, pp. 18–48, 2nd Quart., 2007.
[37] Z. Ping, S. Haoshan, and S. Kui, "The 3D location algorithm based on smart antenna with MUSIC DOA estimates," in *Proc. WRI World Congr. Comput. Sci. Inform. Eng.*, vol. 4, Mar./Apr. 2009, pp. 750–753.
[38] P. Viswanath, D. N. C. Tse, and R. Laroia, "Opportunistic beamforming using dumb antennas," *IEEE Trans. Inf. Theory*, vol. 48, no. 6, pp. 1277–1294, Jun. 2002.
[39] *V2V System Level Performance*, document 3GPP TS R1-155755, Oct. 2015. [Online]. Available: http://www.3gpp.org/

KAIFENG HAN (S'16) received the B.Eng. degree (first-class Hons.) from the Beijing University of Posts and Telecommunications (BUPT) and the Queen Mary University of London (QMUL), in 2015, and the Ph.D. degree from The University of Hong Kong, in 2019, all in electrical engineering. Since August 2019, he has been an Engineer with the Department of Strategic Studies, Institute of Policy and Economics Research, China Academy of Information and Communications Technology (CAICT). His research interests focus on AI, future wireless communications, and autonomous driving.

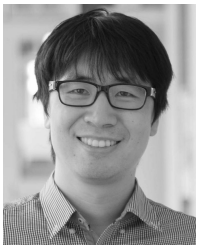

SEUNG-WOO KO (M'17) received the B.S., M.S., and Ph.D. degrees from the School of Electrical and Electronic Engineering, Yonsei University, South Korea, in 2006, 2007, and 2013, respectively. Since March 2019, he has been an Assistant Professor with the Division of Electronics and Electrical Information Engineering, Korea Maritime and Ocean University (KMOU). Before joining KMOU, he has been a Senior Researcher with LG Electronics, South Korea, from March 2013 to June 2014, and a Postdoctoral Researcher at Yonsei University, South Korea, from July 2014 to March 2016, and The University of Kong Kong, from April 2016 to February 2019. His research interests focus on intelligent wireless communications and networking, with special emphasis on edge computing and learning, vehicular positioning, and autonomous driving.

HYUKJIN CHAE received the B.S. and Ph.D. degrees in electrical and electronic engineering from Yonsei University, Seoul, South Korea. From March 2012 to March 2019, he was a professional Research Engineer with the Advanced Standardization Laboratory, LG Electronics. He has participated in 3GPP RAN1 meeting as a delegate, since 2012. He is a Rapporteur of the 3GPP RAN Rel. 15 V2X phase 2 work item. He has published more than 1000 patents in worldwide and more than 100 patents of his patents have been granted in United States. His research interests include interference channels, MIMO, device-to-device (D2D), vehicle-to-everything (V2X), edge computing, machine learning, positioning, and full duplex radio (FDR).

BYOUNG-HOON KIM received the B.S. and M.E. degrees in electronics engineering, and the Ph.D. degree in electrical engineering and computer science from Seoul National University, Seoul, South Korea, in 1994, 1996, and 2000, respectively. From 2000 to 2003, he was with GCT Semiconductor, Seoul, South Korea, developing W-CDMA and WLAN chip sets. From 2003 to 2008, he was with QUALCOMM Incorporated, San Diego, CA, USA, where he was responsible for MIMO technology development and 3GPP LTE standard and design works. Since March 2008, he has been with LG Electronics, currently as the Senior Vice President and the Head of the Advanced Standard Research and Development Lab, developing future technologies and standards for 5G/6G, autonomous driving, Wi-Fi, Bluetooth, the IoT connectivity, as well as advanced broadcasting and media technologies. He has been actively contributing to 3GPP standards for 4G/5G communications and 5GAA standards for connected cars, and he was also involved in the IEEE 802.11ac, 11af, and 11ah standards, and has assumed the role of a member of board of directors of Wi-Fi Alliance during 2011–2012. He is coauthor of the *Scrambling Techniques for CDMA Communications* (Springer, 2001) and was elected as the 1st IEEE Communications Society Asia-Pacific Best Young Researcher, in 2001.

KAIBIN HUANG (S'05–M'08–SM'13) received the B.Eng. (first-class Hons.) and the M.Eng. degrees from the National University of Singapore, and the Ph.D. degree from The University of Texas at Austin (UT Austin), all in electrical engineering. He was a Faculty Member with the Department of Applied Mathematics (AMA), The Hong Kong Polytechnic University (PolyU), and the Department of Electrical and Electronic Engineering (EEE), Yonsei University. He is currently an Associate Professor with the Department of EEE, The University of Hong Kong. His research interests include edge computing and learning and wireless communication techniques. He frequently serves on the technical program committees of major IEEE conferences in wireless communications. He has edited the JSAC 2015 Special Issue on Communications powered by energy harvesting. He received the IEEE Communication Society's 2019 Best Tutorial Paper Award and the 2015 Asia Pacific Outstanding Paper Award, the Outstanding Teaching Award from Yonsei, the Motorola Partnerships in Research Grant, the University Continuing Fellowship from UT Austin, and the Best Paper Awards from the IEEE GLOBECOM 2006 and IEEE/CIC ICCC, in 2018. He was named a Highly Cited Researcher by Clarivate Analytics, in 2019. Most recently, he has served as the Lead Chair for the Wireless Communications Symposium of IEEE Globecom 2017 and the Communication Theory Symposium of IEEE GLOBECOM 2014 and the TPC Co-Chair of the IEEE PIMRC 2017 and the IEEE CTW 2013. He is currently an Associate Editor of the IEEE TRANSACTIONS ON WIRELESS COMMUNICATIONS and the IEEE TRANSACTIONS ON GREEN COMMUNICATIONS AND NETWORKING. He has also served on the editorial boards of IEEE JOURNAL ON SELECTED AREAS IN COMMUNICATIONS (JSAC) series on Green Communications and Networking, and the IEEE WIRELESS COMMUNICATIONS LETTERS.